frontiers in Marine Science

ORIGINAL RESEARCH
published: 27 November 2018
doi: 10.3389/fmars.2018.00450

Relating Coral Skeletal Structures at Different Length Scales to Growth, Light Availability to *Symbiodinium*, and Thermal Bleaching

Timothy D. Swain[1,2], *Simon Lax*[3†], *Natalie Lake*[1], *Hannah Grooms*[1], *Vadim Backman*[4] and *Luisa A. Marcelino*[1,2*]

[1] Department of Civil and Environmental Engineering, Northwestern University, Evanston, IL, United States, [2] Integrative Research Center, Field Museum of Natural History, Chicago, IL, United States, [3] Department of Ecology and Evolution, University of Chicago, Chicago, IL, United States, [4] Department of Biomedical Engineering, Northwestern University, Evanston, IL, United States

OPEN ACCESS

Edited by:
Daniel Wangpraseurt,
University of Cambridge,
United Kingdom

Reviewed by:
Steven L. Jacques,
Tufts University, United States
Robert Ong,
University of Sydney, Australia

***Correspondence:**
Luisa A. Marcelino
l-marcelino@northwestern.edu

†Present Address:
Simon Lax,
Physics of Living Systems,
Department of Physics,
Massachusetts Institute of
Technology, Cambridge, MA,
United States

Specialty section:
This article was submitted to
Coral Reef Research,
a section of the journal
Frontiers in Marine Science

Received: 09 May 2017
Accepted: 08 November 2018
Published: 27 November 2018

Citation:
Swain TD, Lax S, Lake N, Grooms H, Backman V and Marcelino LA (2018) Relating Coral Skeletal Structures at Different Length Scales to Growth, Light Availability to Symbiodinium, and Thermal Bleaching. Front. Mar. Sci. 5:450. doi: 10.3389/fmars.2018.00450

Light scattering of coral skeletons and tissues increases light availability to photosynthetic endosymbionts to form one of the most efficient biological collectors of solar radiation. Rapid increases in light availability during thermally-induced symbiont loss (bleaching) impair photosynthetic performance of the remaining *Symbiodinium* and precipitate a more severe bleaching response (optical feedback-loop hypothesis). Here we focus on light scattering of the skeleton, which is determined by light interaction with skeletal components assembled in a hierarchical fractal-like structure from tens of nanometers (e.g., calcium carbonate nanograins) to micro- and milli-meters (septa, corallites, and coenosteum) to centimeters and higher (colony form). We examined the association between skeletal structures, their role in light scattering, and species-specific bleaching responses for 88 coral species using phylogenetically-corrected analysis. We also explored the effect of growth on light scattering by modeling the fractal-like accretive growth of the skeleton (assuming a diffusion limited process of biomineralization) as a function of skeletal density, size of nanograins, fractal range of biomineralized clusters, and overall mass-fractal dimension, and validated the model with experimental data. Our results show that differences in light scattering from the top ~200 μm (*micro-*μ_s') of the skeleton, and not from the whole skeleton (bulk-μ_s'), are related to bleaching susceptibility. We also demonstrate how differences in *micro-*μ_s' of corallites and coenosteum could explain, in part, the heterogeneous light environment between polyp and coenosarc. The average effective light transport distance of coenosteum measured in 14 coral species indicates that coenosteum could transport light to the corallites, which could then function as "light-trapping devices" where photons are scattered multiple times by septa and corallite walls until absorbed by *Symbiodinium*. Furthermore, our fractal skeletal growth model suggests that corals that grow faster typically have lower mass-fractal dimension, denser skeletons, lower skeletal micro-μ_s', and higher bleaching susceptibility. Finally, our results demonstrate that several skeletal structures of varying

length scales known to modulate the light microenvironment of *Symbiodinium* in coral tissue are not associated with bleaching susceptibility. This work provides evidence of the relationship between skeletal growth, light scattering, and bleaching, and further supports the optical feedback-loop hypothesis of coral bleaching.

Keywords: coral bleaching, light scattering, light transport, optical feedback-loop hypothesis, skeletal growth model

INTRODUCTION

Hermatypic corals are optical machines, adapted for collection of solar energy through complex endosymbioses with photosynthetic dinoflagellates representing the genus *Symbiodinium*. While the basic components of these machines are simple to envision, a thin layer of largely transparent tissue that suspends solar collectors over a light-scattering surface, the diversity of interacting forms and functions are complex. Structural components, and the interactions between components, combine to maximize photosynthesis while simultaneously minimizing photo-damage to their symbionts and themselves. Optimization of these functions has derived a diversity of forms that make corals some of the most efficient biological collectors of solar radiation (Enríquez et al., 2005, 2017; Brodersen et al., 2014), and allows them to occupy habitats characterized by diverse light conditions ranging over two orders of magnitude from the intense solar irradiances of reef crests to near darkness of mesophotic reefs (Anthony and Hoegh-Guldberg, 2003; Pochon et al., 2015). However, light collection optimization in corals comes with a cost when thermal anomalies induce disruption of coral-*Symbiodinium* symbioses (bleaching), which has become an urgent focus of research as global temperatures continue to increase under climate change (Hoegh-Guldberg et al., 2007; Baker et al., 2008; Frieler et al., 2013; Hughes et al., 2017). Thermal stress impairs function of the photosynthetic apparatus of *Symbiodinium* (Iglesias-Prieto et al., 1992; Warner et al., 1999), reducing the light intensity threshold for bleaching (Mumby et al., 2001; Bhagooli and Hidaka, 2004; Lesser and Farrell, 2004). *Symbiodinium* photosynthesis is the primary source of fixed carbon for reef-building corals (Muscatine, 1990), and loss of *Symbiodinium* during bleaching may lead to mortality of the holobiont (Jokiel, 2004; Jones, 2008). This increased sensitivity to light may be determined, in part, by the same mechanisms responsible for modulating the internal light environment that allow corals to inhabit such diverse light regimes.

Increase in light availability to *Symbiodinium* is modulated by the coral host through multiple scattering in the coral skeleton and tissue (Kühl et al., 1995; Enríquez et al., 2005, 2017; Stambler and Dubinsky, 2005; Terán et al., 2010; Marcelino et al., 2013; Wangpraseurt et al., 2016) and through dynamic light redistribution due to tissue contraction and expansion (Wangpraseurt et al., 2012, 2014a; Lichtenberg et al., 2016), as well as light scattering or absorption by host fluorescent pigments (Salih et al., 2000; Lyndby et al., 2016). Fluorescent pigments in coral tissues have been shown to affect light absorption, scattering, and heating (Lyndby et al., 2016), while also reducing the harmful effects of short-wavelength radiation and providing photoprotection through light absorption (Schlichter et al., 1986; Salih et al., 2000; Lesser and Farrell, 2004; Smith et al., 2013).

Here we focus on modulation of light microenvironment by the skeleton, which is dependent on the ability of light to reach the skeleton (i.e., >95% of downwelling or tissue-scattered irradiance is absorbed by *Symbiodinium*; e.g., Magnusson et al., 2007) and the diffuse reflectance of the skeleton (i.e., scattering properties of skeletal material determined by the interaction of light with skeletal structures; Kühl et al., 1995; Enríquez et al., 2005, 2017; Stambler and Dubinsky, 2005; Terán et al., 2010; Kahng et al., 2012; Marcelino et al., 2013; Wangpraseurt et al., 2017). Skeletal reflectance has been shown to increase light availability to *Symbiodinium* in tissue up to six times (depending on the concentration of symbiont cells) relative to cultures (Kühl et al., 1995; Enríquez et al., 2005). This observation lead to the optical feedback-loop (or positive feedback-loop) hypothesis of coral bleaching: as symbionts and/or their pigments are lost in the initial stages of a bleaching event, the reduction of light absorbers further exposes the skeleton, which disproportionately increases excess light availability to the remaining *Symbiodinium*, causing greater symbiont loss and acceleration of the bleaching response (Enríquez et al., 2005; Marcelino et al., 2013; Swain et al., 2016b). Skeletal reflectance is influenced by overall morphology, light absorption, and light scattering. Light scattering is characterized by the reduced scattering coefficient, bulk-μ_s' or μ_s', which is the inverse distance a photon travels before it is randomized in direction (i.e., transport mean free path length, $l_s' = 1/\mu_s'$; Anthony et al., 2005; Enríquez et al., 2005; Stambler and Dubinsky, 2005; Rodríguez-Roman et al., 2006; Marcelino et al., 2013). Light is scattered by interacting with skeletal structures ranging from ∼30–100 nm (e.g., $CaCO_3$ nanograins; Stolarski, 2003; Cuif and Dauphin, 2005a) to ∼1–10 mm (e.g., corallites and septa; Enríquez et al., 2005; Stambler and Dubinsky, 2005) to ∼1–10 cm or more (Enríquez et al., 2005; Stambler and Dubinsky, 2005; Wangpraseurt et al., 2017; e.g., corallite walls and coenosteum).

Skeletal light scattering in the top ∼200 μm superficial layer of the skeleton has been described as microscopic-μ_s' or $\mu_{s,m}'$ (Rogers et al., 2009; Marcelino et al., 2013) and is primarily affected by skeletal microstructures, but not larger features or voids known to affect bulk-μ_s' (Marcelino et al., 2013). Skeletal $\mu_{s,m}'$ is highly variable among coral species and inversely correlated to their bleaching responses (Marcelino et al., 2013). This relationship has been hypothesized to be due to the inverse relationship between $\mu_{s,m}'$ and the *rate of excess light increase* in coral tissue as symbionts are lost, as demonstrated

by physical models of simulated bleaching (Marcelino et al., 2013). The inverse dependence of bleaching response on $\mu_{s,m}{}'$ was also observed experimentally among ten coral species (while differences in *Symbiodinium* thermotolerance and host tissue thickness were insufficient to explain differential bleaching; Swain et al., 2016b). Microscopic-$\mu_s{}'$ was also shown to be capable of modulating a 2- to 5-fold increase in light absorption per unit pigment in *Symbiodinium* when modeling skeleton-dependent light absorption (Swain et al., 2016b). These observations lead to the prediction that $\mu_{s,m}{}'$ is responsible for the rate of optical feedback, where corals with low-$\mu_{s,m}{}'$ may scatter less light to *Symbiodinium*, however once thermally-induced bleaching reduces absorber concentrations in the tissue, low-$\mu_{s,m}{}'$ corals have higher rates of light increase to its symbionts resulting in compounded stress and accelerated bleaching (Marcelino et al., 2013; Swain et al., 2016b). Skeletal optical feedback was also demonstrated with direct micro-sensor measurements of light within live coral tissue, which detected up to a 5-fold enhancement of light directly above the skeleton of bleached corals (relative to healthy corals) at a rate of increase that approximated a power-law function relative to decreasing *Symbiodinium* densities (Wangpraseurt et al., 2017).

Coral skeletons, similar to other biominerals (e.g., mollusk nacre, bone, or glass sponge spicules; Kamat et al., 2000; Aizenberg et al., 2005; Benzerara et al., 2011), contain 30–100 nm calcium carbonate crystals (orthorhombic structure aragonite) assembled in a hierarchical fractal-like structure. These structures spanfrom nanometer–scale interactions between calcium carbonate grains and organic matrix, to micrometer–scale associations of crystal fibers forming "thickening deposits" between "centers of calcification" (COC), to millimeter–scale assemblies of septa in corallites, to overall colony formation (Stolarski, 2003; Cuif and Dauphin, 2005a,b; Stolarski and Mazur, 2005; Nothdurft and Webb, 2007; Przeniosło et al., 2008; Benzerara et al., 2011). Recent observations suggest that skeletal organic matrix (SOM) found in the COCs works as an organic substrate where nanoparticles of amorphous calcium carbonate (40–50 nm in diameter) are deposited and combine to form aragonite crystals that lead to the formation of the skeletal fibers (Von Euw et al., 2017). This process of crystal formation, designated as crystallization by particle attachment (CPA), has been observed to occur in biomineralized materials, such as sea urchin spicules or zebrafish fin bone, and could be due, in part, to diffusion-limited kinetics (De Yoreo et al., 2015). In corals, accretion of aragonite nanograins in the skeleton is a diffusion-limited process, dependent on the secretion of ions (calcium, carbonate, and protons) and organic matrix molecules (involved in crystal nucleation) by specialized cells in the basal ectoderm of the coral tissue (calicoblastic cells), and occurs through a combination of linear extension and thickening (Stolarski, 2003; Cuif and Dauphin, 2005b; Nothdurft and Webb, 2007; Frankowiak et al., 2016). Growth of fractal-like structures can be described by mass-fractal dimension, or D_f , which characterizes the overall size distribution of skeletal structural elements at different length scales (Basillais, 1997; Martin-Garin et al., 2007; Przeniosło et al., 2008; Young et al., 2017). In the case of branching corals, D_f has been hypothesized to reflect their optimal growth strategies along gradients of light and nutrient-flow that result in high morphological plasticity (Kaandorp et al., 2005; Chindapol et al., 2013). Skeletal D_f was shown to be highly correlated with skeletal $\mu_{s,m}{}'$ in 94 coral taxa (Marcelino et al., 2013).

Furthermore, several skeletal structures have been implicated in light collection due to light-induced morphological plasticity. Corallite morphology and spacing among corallites can be plastic in response to differing light environments. Calices can become deeper and septa shorter (Todd et al., 2004; Ow and Todd, 2010), corallite diameter smaller (Nir et al., 2011), and three-dimensional topography of calice surfaces (calical relief) greater (Klaus et al., 2007) under higher radiation. Distances among corallites may increase and corallite surface area decrease under higher radiation (Nir et al., 2011) or change under different spectral conditions (Rocha et al., 2014). There are also differences in light enhancement observed during bleaching in polyp (above corallites) and coenosarc (above coenosteum) tissues, with greater enhancement above the more structurally complex corallites (Wangpraseurt et al., 2017).

At longer length scales, colony morphology is known to change dramatically within some coral species across light (with colony form becoming less compact; Muko et al., 2000; Kaniewska et al., 2008; Todd, 2008) and nutrient-flow gradients (e.g., Smith and Birkeland, 2007; Jimenez et al., 2011; Chindapol et al., 2013), and to be highly diverse between species (e.g., plating, massive, branching, etc.). Internal light fields within tissues have been shown to vary across different colony morphologies and between coenosarc and polyps (Wangpraseurt et al., 2014b). Additionally, differential bleaching among various morphologies has been extensively reported, with massive and encrusting forms thought to be generally more resistant to bleaching then branching and digitate forms (e.g., Marshall and Baird, 2000; Loya et al., 2001; van Woesik et al., 2011; but see McCowan et al., 2012; Swain et al., 2018).

Here we evaluated the role of skeletal structures in light scattering, examined the effect of skeletal growth on light scattering, and tested the effect of coral skeletal structures and traits on bleaching response with the goal of identifying individual or groups of skeletal structures that could be predictive of bleaching susceptibility. Specifically, we evaluated (1) if high variability in light microenvironments within a colony, especially between coenosarc (over coenosteum) and the polyp (over corallite) tissues which yield different photosynthetic efficiencies (Ralph et al., 2002; Ulstrup et al., 2006, 2007; Wangpraseurt et al., 2017), could be partially explained by differences in skeletal $\mu_{s,m}{}'$ between the coenosteum and corallites; (2) the relationship between skeletal features and bleaching response of 88 coral species by performing phylogenetically-corrected regression analysis with overall skeletal architecture (mass-fractal dimension, D_f), colonial unit dimensions (corallite diameter) and organization (corallite complexity and coenosteum surface area), and colony structure (cumulative fractality); and (3) the effect of skeletal growth on light scattering and bleaching susceptibility by modeling the relationship between skeletal density (n), D_f, and growth rate.

METHODS

Coral skeletal characters were collected from museum specimens, literature, or trait databases (values and their sources reported in **Table S1** and **Text S1**), and their relationship to bleaching response was assessed through phylogenetically corrected regression and principal components analyses. Out of 95 coral taxa previously characterized for bleaching response (Swain et al., 2016a), microscopic-μ_s', and mass-fractal dimension D_f by Marcelino et al. (2013), we retained the 88 that were identified to species such that further species-specific data could be applied to these analyses. Bleaching response values for species not reported, or with fewer than three observations, in Swain et al. (2016a) were taken as the mean of responses across the genus (**Table S1**).

Character Collection

Characters related to skeletal light scattering and micro-architecture of the skeleton are described below; the remaining characters are described here. **Skeletal density (*n*)**, the maximum mass of skeletal material per cubic cm ($g{\cdot}cm^{-3}$), is affected by skeletal extension and thickening of nanograins (Bucher et al., 1998) and species-specific values were either obtained from the literature or directly measured from museum specimens of Marcelino et al. (2013) using standard methods (mass divided by volume determined by displacement of water; Hughes, 1987). Species-specific **skeletal growth rate** values, characterized by the maximum linear increase in skeleton deposits measured over a year ($mm{\cdot}yr^{-1}$), were obtained from the literature and related to n and D_f by a coral growth model (see equations 9–13). Species-specific corallite arrangement (**corallite size** measured as corallite max diameter, corallite complexity, and percent of surface area composed of coenosteum) were also obtained. **Corallite complexity**, was parameterized by counting the number of septa within each cycle, and weighing septal counts within cycles by their extension from the corallite wall toward the columella (sum of the number of septa per cycle · extension weight) within 10 corallites for each species from the museum specimens of Marcelino et al. (2013). Primary septal cycles (i.e., those that extend to the columella) were weighted by a factor of three, intermediate cycles were weighted by a factor of two, and cycles that extend minimally from the corallite wall were unweighted. The percent of surface area composed of coenosteum (**% $SA_{coenosteum}$**) was parameterized through direct measurements of museum specimens of Marcelino et al. (2013) captured in size-standardized digital photos and subtracting the area occupied by corallites from the total area of skeletal surface in photographs using ImageJ (version 1.47; NIH). Colony growth morphology was estimated by calculating **cumulative fractality** for each of 10 growth forms characterizing the 88 coral species, which is the product of *apparent surface fractality* of the colony and mass-fractal dimension D_f. *Apparent surface fractality* was measured by visually scoring the structural complexity (i.e., rugosity, or the 3D surface area occupying a given volume) of individual specimens representing each growth form such that encrusting forms were scored the lowest given their low surface area per volume ratio and branching forms (especially closed branches) were scored the highest (modified from Young et al., 2017).

Differential Light Scattering of Coral Skeletal Components

Bulk skeletal scattering (bulk-μ_s', characterized by the reduced light scattering coefficient μ_s' measured in mm^{-1}), is the inverse distance a photon travels before it is randomized in direction, and results from light interaction with voids and skeletal structures at different length scales throughout the entire skeleton (Enríquez et al., 2005; Stambler and Dubinsky, 2005; Terán et al., 2010). **Micro-skeletal light scattering** (micro-μ_s' or $\mu_{s,m}'$) is the reduced light scattering coefficient within the top ∼200 μm of the skeleton and is not influenced by voids (Marcelino et al., 2013; Swain et al., 2016b). Micro-μ_s' was measured using low-coherence enhanced backscattering spectroscopy (LEBS) on tissue-free coral skeletons. The LEBS instrument and principles were described in detail by Marcelino et al. (2013) and references therein, but briefly, LEBS can measure microscopic light-scattering through broadband partial spatial coherence of illumination (*Lsc*) which selectively isolates the scattering spectrum from photons that propagate paths such that the distance between light entry and light exit points is comparable to *Lsc*.

Measurements of $\mu_{s,m}'$ of corallites and coenosteum were taken for a subset of 14 species (previously characterized for skeletal $\mu_{s,m}'$ at the colony level by Marcelino et al., 2013), with corallite diameters and distances between corallites (i.e., coenosteum) larger than the instrument spot size (∼1 mm in diameter). Their ratio was calculated as,

$$\mu_{S,m\_Ratio}{}' = \frac{\mu_{S,m,\ corallite}{}'}{\mu_{S,m,\ coenosteum}{}'} \quad (1)$$

Values for $\mu_{s,m\_corallite}{}'$ and $\mu_{s,m\_coenosteum}{}'$ are reported as the means of ten replicate measurements. To evaluate the potential for coenosteum to transport light into adjacent corallites, we calculated the effective light transport distance of coenosteum ($ETD_{coenosteum}$), which measures how much light can be transported by coenosteum given its intrinsic $\mu_{s,m}'$ (and therefore transport mean free path length, $l'_{S,m} = 1/\mu_{s,m}'$) and inter-corallite distance ($D_{inter-corallite}$) such that:

$$ETD_{coenosteum} = \frac{D_{inter-corallite}}{l_{s,m}{}'} \quad (2)$$

where $l'_{S,}$and $D_{inter-corallite}$ are measured in millimeters. A high $ETD_{coenosteum}$ value indicates low potential for coenosteum to transport light into adjacent corallites. $D_{inter-corallite}$ is the mean distance between ten haphazardly chosen adjacent corallites captured in size-standardized digital photos of the museum specimens of Marcelino et al. (2013), extracted using ImageJ (version 1.47; NIH).

Modeling of Irradiance at the Corallite Surface

The effect of light transport in the coenosteum on corallite irradiance was modeled based on the diffusion approximation to

the light transport equation (Zonios et al., 1999). Corallites were approximated as semi-infinite axially-symmetrical cylindrical regions of turbid media, surrounded by semi-infinite regions of coenosteum, with the scattering properties measured by LEBS. In this approximation, irradiances relative to the incident intensity that would be observed at the surface layer of the corallite (R_1) and the coenosteum (R_2) regions due to a uniform illumination of the coral surface are, respectively,

$$R_1(r) = \int_0^{r_c} \int_0^{2\pi} R\left(\sqrt{r^2 + r'^2 - 2rr'cos\phi};\, \mu'_{s1}, \mu_{a1}\right) r'\, d\phi\, dr' \tag{3}$$

where r is the radial distance from the center of the corallite, r_c is the radius of the corallite, μ'_{s1} and μ_{a1} are the reduced scattering and the absorption coefficients of the corallite, respectively, and $R(x; \mu'_s, \mu_a)$ is the irradiance observed at a distance x from a point source at a surface of a semi-infinite slab of turbid media with the reduced scattering and absorption coefficients μ'_s and μ_a, respectively. The point-source reflectance is derived from the diffusion approximation as follows from Zonios et al. (1999):

$$R_{(\lambda,r)} = \frac{z_0}{4\pi} \frac{\mu_s'}{\mu_s' + \mu_a} \left[\left(\mu + \frac{1}{r_1}\right) \frac{\exp(-\mu r_1)}{r_1^2} + \left(1 + \frac{4}{3}A\right) \left(\mu + \frac{1}{r_2}\right) \frac{\exp(-\mu r_2)}{r_2^2} \right] \tag{4}$$

with

$$\mu = \left[3\mu_a(\mu_a + \mu_s')\right]^{1/2};\ z_0 = \frac{1}{\mu_s' + \mu_a};\ r_1 = \left(z_0^2 + r^2\right)^{1/2};$$
$$r_2 = \left[z_0^2 \left(1 + \frac{4}{3}A\right)^2 + r^2 \right]^{1/2}$$

Some light illuminating the corallite at any given point gets diffusely scattered within the corallite and returns to its surface after which it leaves the coral. A portion of the light, however, may reach the coenosteum region and reach the surface of the coenosteum after being multiply scattered in that region. This irradiance is modeled as the result of the diffusion of light reaching the outer radius of the corallite:

$$R_{1\to 2}(r) = R_1(r_c) \frac{\int_0^{2\pi} R\left(\sqrt{r^2 + r'^2 - 2rr'cos\phi};\, \mu'_{s2}, \mu_{a2}\right) d\phi}{\int_0^{2\pi} R\left(2r_c\sqrt{1 - cos\phi};\, \mu'_{s2}, \mu_{a2}\right) d\phi} \tag{5}$$

where μ'_{s2} and μ_{a2} are the reduced scattering and the absorption coefficients of the coenosteum.

Similarly, the surface irradiance relative to the illumination intensity in the coenosteum region due to the illumination of the coenosteum is

$$R_2(r) = \int_{r_c}^{r_c + L/2} \int_0^{2\pi} R\left(\sqrt{r^2 + r'^2 - 2rr'cos\phi};\, \mu'_{s2}, \mu_{a2}\right) r'\, d\phi\, dr' \tag{6}$$

where L is the average intercorallite distance, and the irradiance of light that is transported from the coenosteum and reaches the corallite surface is

$$R_{2\to 1}(r) = R_2(r_c) \frac{\int_0^{2\pi} R\left(\sqrt{r^2 + r'^2 - 2rr'cos\phi};\, \mu'_{s1}, \mu_{a1}\right) d\phi}{\int_0^{2\pi} R\left(2r_c\sqrt{1 - cos\phi};\, \mu'_{s1}, \mu_{a1}\right) d\phi} \tag{7}$$

Taken together, the irradiance in each of the two regions, corallite and coenosteum, has two components: the "endogenous" light due to the illumination of the specific region and the light transported from the other region:

$$R(r) = \begin{cases} R_1(r) + R_{2\to 1}(r), & r < r_c \\ R_2(r) + R_{1\to 2}(r), & r \geq r_c \end{cases} \tag{8}$$

Micro-Architecture Organization of the Skeleton

Skeletal Mass-Fractal Dimension (D_f)

Micro-skeletal structures of different sizes vary in micro-density and these variations in density, which give rise to light scattering, result in different refractive indices (Kim et al., 2004; Rogers et al., 2009, 2014). Since optical refractive index is linearly dependent on local mass density, the overall organization of structures with size r between ~30–1,000 nm can be characterized by the optical refractive index correlation function C(r) (Kim et al., 2004; Rogers et al., 2009, 2014). LEBS measures fractal-dimension D_f, which quantifies the shape of C(r) (Marcelino et al., 2013). D_f was measured for all 88 species and determined to be consistent with a "mass-fractal" structure (i.e., $D_f < 3$) and varied significantly between low- and high-$\mu_{s,m}{}'$ corals (Marcelino et al., 2013).

Relating Skeletal Density and Fractal-Like Skeletal Organization to Growth Rate

Skeletal growth can be expressed as a function of (1) the size of the elementary unit block (nanograin), which has been observed between 30 and 100 nm in a few species using atomic force microscopy (Cuif and Dauphin, 2005a) and 40–50 nm in *Stylophora pistillata* using scanning helium ion microscopy (Von Euw et al., 2017), and its density (assumed to be 2.73 g/cm^3 or the density of calcium carbonate), (2) the size of larger clusters as biomineralization occurs over different length scales through a mass-fractal equation of crystal growth (Uwaha and Saito, 1990; Peitgen et al., 1992; Miyashita et al., 2005), and (3) the distance between the cellular release of ions (e.g., calcium, carbonate and protons) and organic matrix molecules by calicoblastic cells and their incorporation into the mineralization site (incorporation diffusion length, l) assuming a diffusion-limited process (Furukawa et al., 2001; Allemand et al., 2004).

$$M = M_{\min} \left(\frac{R}{r}\right)^{D_f} \tag{9}$$

$$n = \frac{M}{V} = \frac{M_{\min}}{r^{D_f} R^{3-D_f}} = \left(\frac{r}{R}\right)^{3-D_f} n_0 \tag{10}$$

$$\frac{n}{n_0} = \left(\frac{r}{R}\right)^{3-Df} \tag{11}$$

where, M represents the mass of a biomineralized fractal cluster, M_{min} represents the mass of the elementary unit block (i.e., nanograin), D_f is the mass-fractal dimension of the coral skeleton, r represents radius of the nanograin, R represents the radius of a biomineralized cluster (possibly the "mesocrystals"; domains in "calcification centers" of *Porites sp* skeletons consisting of nanograins organized crystallographically as one large crystal over several micrometers; Benzerara et al., 2011), n represents the average skeletal density, V is the volume of the fractal cluster, and $n_0 = \frac{M_{\min}}{r^3}$ represents the density of the nanograin. Incorporation diffusion length l, (Furukawa et al., 2001) can be expressed as:

$$l = 2Diff/G \tag{12}$$

where, $Diff$ is the diffusion coefficient of the ions and other elements involved in the mineralization process and G is the growth rate (interface velocity or the rate of linear increase of the skeletal surface at the deposition interface). Since the radius of a cluster R should be half the diffusion length (Uwaha and Saito, 1990; Furukawa et al., 2001; Miyashita et al., 2005), then:

$$R = \frac{1}{2}l => R = \frac{Diff}{G} => G \propto \frac{1}{R} \propto \left(\frac{n}{n_0}\right)^{\frac{1}{3-D_f}} \tag{13}$$

Since $D_f < 3$ (Furukawa et al., 2001), it follows that denser skeletons (i.e., higher n) tend to grow faster than less dense skeletons and the relationship between G and n is a power-law with an exponent depending on D_f.

In order to test these model predictions, we used previously measured mass-fractal dimension D_f values for the 88 targeted species. The data showed that the majority of coral skeletons had $D_f < 3$ (Marcelino et al., 2013; see **Text S2**). This implies that the density auto-correlation function typically follows an inverse power-law relationship, between the minimal length scale r and the maximal length scale R, thus supporting the notion that coral skeletons are mass fractal-like structures. We tested the experimental relationship between growth rate G (characterized by maximum linear extension rates of species-specific skeletons), skeletal density n, and D_f, of each skeleton and compared it to the relationship obtained by the model (equation 13). Using available datasets and literature we compiled species-specific (1) maximum linear extension rates of skeleton ($mm \cdot yr^{-1}$) as a proxy for growth rates and (2) maximum skeletal density values ($g\ CaCO_3 \cdot cm^{-3}$) (**Table S1**).

Phylogenetic Statistical Analyses

Coral species characters were mapped onto a molecular phylogeny for assessment of homoplasy, phylogenetically-corrected regression, and phylogenetically-corrected principal components analysis. Patterns among species traits may be determined by a combination of ecological and evolutionary processes, and the ecological process can only by accurately assessed once the patterns of shared evolutionary history are accounted for (Rezende et al., 2007; Ivens et al., 2016). The patterns of shared evolutionary history violate an assumption of standard statistical analyses that individual data points are independent, and must be corrected for phylogeny (Revell, 2010). The comprehensive coral phylogeny of Huang (2012) was trimmed to include only the targeted species, the 88 species tree and a 14 species sub-set tree, using the Phylotools R package (Revell, 2012) to preserve proper branch lengths. These trimmed phylogenetic trees were used to define the evolutionary relationships and distances between species for phylogenetic correction of the raw data.

Characters were mapped onto the trimmed Huang (2012) phylogenies using Mesquite 2.75 (Maddison and Maddison, 2011) and visualized with Evolview (Zhang et al., 2012). Homoplasy of categorical data were assessed through the Retention Index (RI) in Mesquite, which is the fraction of apparent synapomorphy (character present in ancestor and shared exclusively by its evolutionary descendants) retained after mapping to the phylogeny, where highly homoplasious characters have low RI values (Farris, 1989). Relationships between continuous variables were assessed with Phylogenetic Independent Contrasts (PIC) analysis within the Phenotypic Diversity Analysis Programs (PDAP) of Mesquite, which corrects an ordinary least squares linear regression for non-independence due to evolutionary relationships among species (Midford and Garland, 2010). We report the results of phylogenetic independent contrasts through the Pearson Product-Moment Correlation Coefficient, or PCC, as well as its p-value. Skeletal features that were not found to be associated with bleaching response through PIC analyses were further assessed to determine if combinations of these features could be correlated with bleaching. Phylogenetically-corrected linear combinations of skeletal features were identified through phylogenetic principal component analysis (phylo-PCA) (Revell, 2009) using the Phytools R package (Revell, 2012). Phylogenetically corrected logistic regressions (Ives and Garland, 2010) of dichotomous variables (branching/massive colony morphology) were performed in Phyloglm v2.4 (Phylogenetic Generalized Linear Model; Ho and Ané, 2014) in R. Because of incomplete taxon sampling for n and G, and the order of magnitude greater parameters for solitary species (which made them extreme outliers in our analyses), the taxa included in the phylo-PCA were reduced to 59 species (**Table S1**). Phylo-PCAs were based on variable correlation rather than covariance due to their vastly different distributions. Principal components are reported in non-corrected space, therefore assessment of correlation with bleaching response was performed with PIC as above.

RESULTS AND DISCUSSION

Skeletal light scattering, which increases the light microenvironment of *Symbiodinium* in coral tissue and accelerates bleaching response (Enríquez et al., 2005; Marcelino et al., 2013; Swain et al., 2016b; Wangpraseurt et al., 2017), is due to light interaction with structures varying in size from tens of nanometers (30–100 nm calcium carbonate nanograins) to micrometers and millimeters (corallite septa and walls) or higher

(coenosteum and colony morphology; Enríquez et al., 2017). Here we evaluated skeletal structures at length scales spanning seven orders of magnitude that are known to affect within-tissue light environment and their relationship with light scattering and bleaching response of 88 coral species. We also modeled the interaction between skeletal growth rate and skeletal density given the fractal-like accretive growth of the skeleton and its potential association with bleaching.

Differences in Skeletal Micro-μ_s', and Not in Bulk-μ_s', Are Related to Bleaching Susceptibility

Bleaching responses of the 88 targeted coral species are highly diverse (bleaching response index, taxon-BRI, ranged from 2.75 to 72.85%, Swain et al., 2016a) and appear to have multiple independent evolutionary origins (i.e., bleaching response is homoplasious across the phylogeny resulting in a low RI = 0.33, **Figure 1**), providing an opportunity to detect correlations with skeletal characters that may otherwise closely reflect evolutionary history. Homoplasious characters provide a better opportunity to reveal the underlying relationships between character states, after correction for phylogenetic non-independence (Revell, 2010) among species.

The pattern of increased taxon-BRI associated with decreased $\mu_{s,m}'$ (Phylogenetic independent contrast tests, PCC = −0.24, $p = 0.024$, $n = 88$; **Figure 1**; **Table S2**), is consistent with earlier work of our lab (Marcelino et al., 2013) and supports the optical feedback-loop hypothesis (Enríquez et al., 2005; Marcelino et al., 2013; Swain et al., 2016b; Wangpraseurt et al., 2017). This pattern is robust to decreased sample size (88, rather than 95 taxa), increased precision of the phylogeny used for correction of non-independence (using the updated and more comprehensive phylogeny of Huang, 2012), and increased precision of the species-specific estimation of bleaching response (using the updated and more comprehensive bleaching response values of Swain et al., 2016a). Association with bleaching response is specific to the light-scattering properties within the top ∼200 μm of the coral skeleton ($\mu_{s,m}'$) and was not detected in the light scattering properties within the overall skeleton (bulk-μ_s', PCC = 0.06, $p = 0.708$, $n = 42$), mirroring our earlier findings using 10 experimentally bleached coral species (Swain et al., 2016b).

While we cannot currently explain these patterns, we hypothesize that they may be due, in part, to significant structural and chemical differences between the top ∼200 μm layer and the rest of the skeleton. Separation between the most recently deposited biomineral and older parts of the skeleton is made by exothecal dissepiments; thin horizontal plates of biomineralized calcium carbonate laid as the colony extends upwards which varies among species. Dissepiment spacing was measured at 60–460 μm in *Porites lobata*, 180–720 μm in *Goniastrea favulus*, 200–1,000 μm in *Pocillopora damicornis*, (overall mean of ∼400 μm; Nothdurft and Webb, 2007), 550–620 μm in *Orbicella annularis* and *Montastrea faveolata*, 800–850 μm in *Montastrea cavernosa*, and 680–720 μm in *Montastrea franski* (overall mean of ∼600 μm; Dávalos-Dehullu et al., 2008). Micro-μ_s' may result from light scattering by the most recently biomineralized calcium carbonate and organic matrix located above the latest dissepiment (e.g., the >60 nm voids in *Goniastrea stelligera* skeleton; Frankowiak et al., 2016), while bulk-μ_s' would result from light scattering by new and old skeleton where older voids could potentially be filled with water or gas due to degradation of organic material. However, how the structural and chemical composition of the top skeletal layer is associated with bleaching susceptibility will require further investigation.

Differences in Skeletal Micro-μ_s' of Corallites and Coenosteum Explain, in Part, Heterogeneous Light Environment Between Polyp and Coenosarc and Are Associated With Bleaching Susceptibility

Differential photosynthetic efficiencies between polyp (above corallite) and coenosarc (above coenosteum) tissues have been attributed to high variability in within-colony light environments (Kühl et al., 1995; Ralph et al., 2002; Ulstrup et al., 2006, 2007). We reasoned that this high variability could be explained, in part, by differences in skeletal light scattering and transport between corallites and coenosteum. To that effect, we first measured light scattering properties and morphometrics of corallites and coenosteum in 14 coral species and then modeled the irradiance that reaches the corallite from coenosteum-transported light in three coral species with differing efficacy of light transport.

We measured $\mu_{s,m}'$ of corallites ($\mu_{s,m\_corallite}'$) and coenosteum ($\mu_{s,m\_coenosteum}'$), calculated their ratio (μ_{S,m_Ratio}', Equation 1) and determined the effective light transport distances of coenosteum ($ETD_{coenosteum}$) for 14 coral species (**Figure 2**). The $ETD_{coenosteum}$ (equation 2), corresponds to the probability that light that enters the coenosteum could be diffusely transported into a corallite and is dependent on the distance traveled by a photon before scatter and randomization (transport mean free path in the top ∼200 μm of the skeleton, $l_S'_m$, where $l'_{S,m} = 1/\mu_{s,m}'$), and on the mean inter-corallite distance ($D_{inter-corallite}$) within a colony. A high $ETD_{coenosteum}$ indicates low probability that light entering coenosteum will be transported to neighboring corallites; similarly to within-tissue transport, the coenosteum could effectively transport light into corallites with inter-corallite distances up to ∼20× $l_S'_{m\_coenosteum}$, (Ishimaru, 1999). In corals with ($\mu_{s,m\_corallite}'/\mu_{s,m\_coenosteum}'$) > 1, and $D_{inter-corallite}$ < 20× $l_S'_m$, the coenosteum could transport light to corallites which could then work as "light-trapping devices" where photons could be scattered multiple times by corallite septa and walls until absorbed by *Symbiodinium*. The 14 corals examined had (mean ± standard deviation) $l_S'_{m\_coenosteum} = 0.24 \pm 0.12$ mm; $D_{inter-corallite} = 2.3 \pm 1.8$ mm; $ETD_{coenosteum} = 13.48 \pm 12.97$ and $\mu_{S,m\_Ratio}' = 1.11 \pm 0.33$, indicating that coenosteum could effectively transport light into corallites and be trapped by multiple scattering. Accordingly, corals with low-scattering coenosteum and high scattering corallites that are spaced within effective transport distances would be more likely to increase light availability to their *Symbiodinium* and precipitate a more rapid bleaching response under increased thermal

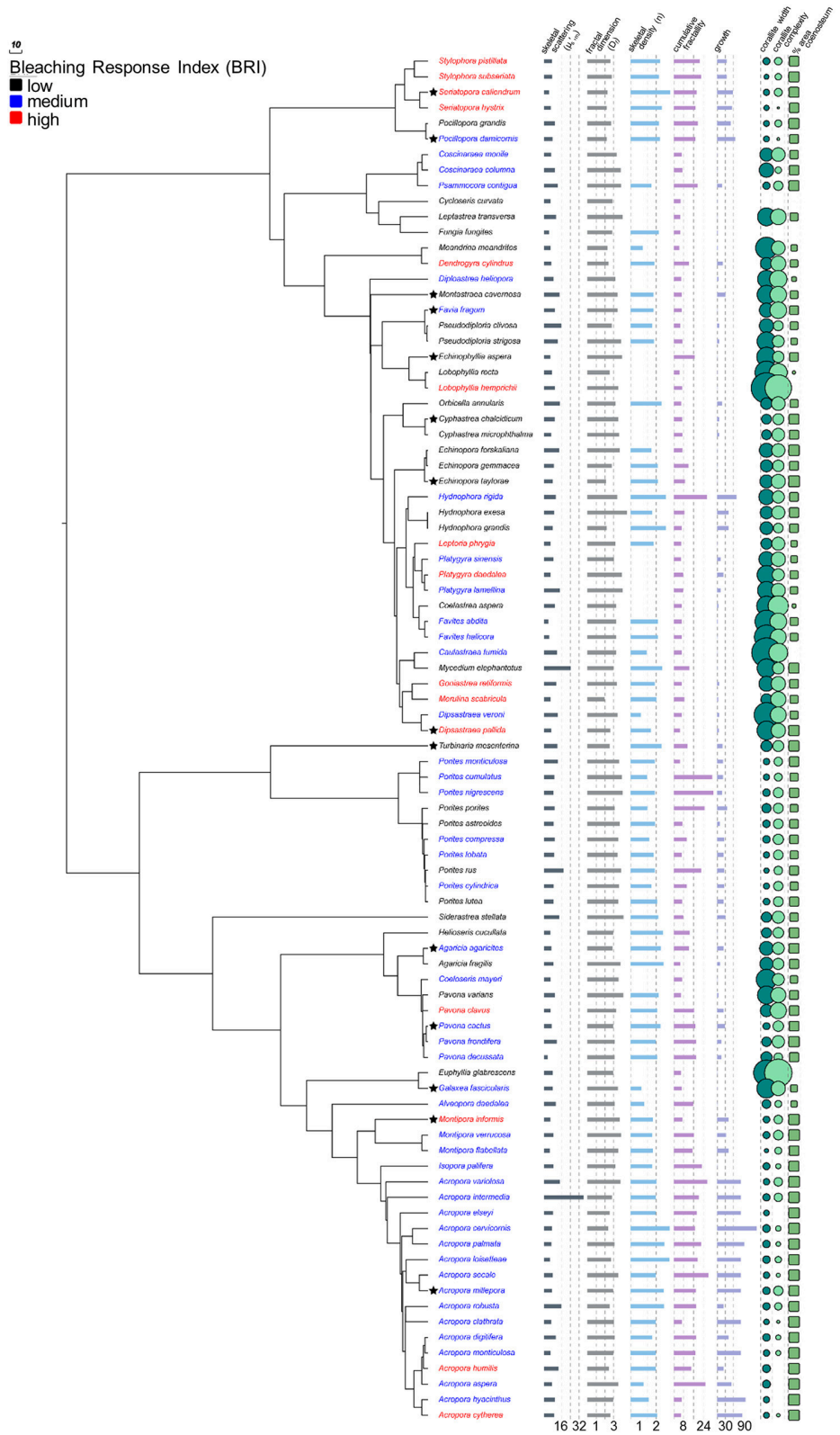

FIGURE 1 | Coral phylogeny of 88 species modified from Huang (2012) with skeletal characters. Coral species color coded by bleaching response and bar graphs, circular plots, and rectangular plots represent variation in skeletal characters. Values for *Cycloseris curvata* and *Fungia fungites* are omitted from circular plots as they are an order of magnitude larger than all other species (see **Table S1**). Stars indicate species for which additional $\mu_{S,m}{}'$ data were collected for corallites and coenosteum. Lower $\mu'_{S,m}$ values are associated with increased bleaching response (PCC $= -0.24$, $p = 0.024$), but other characters are not. See **Figure 5** for phylogenetic principal components analysis of non-light-scattering characters and **Table S2** for complete phylogentic regression analysis of all characters.

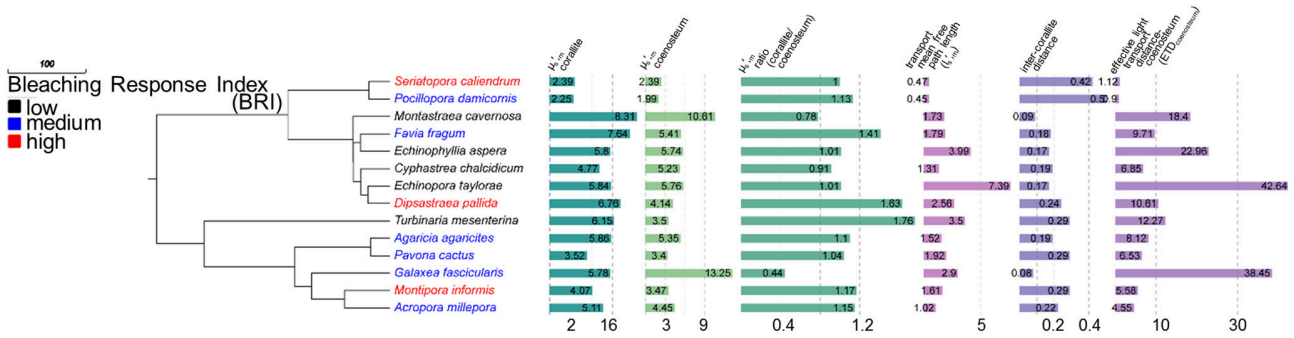

FIGURE 2 | Coral phylogeny of 14 species modified from Huang (2012) with isolated skeletal scattering ($\mu_{s,m}'$) values for corallites and coenosteum. Coral species color coded by bleaching response and bar graphs represent variation in skeletal characters. Higher corallite $\mu_{s,m}'$ values, relative to coenosteum, are associated with increased bleaching response (PCC = 0.69, $p = 0.006$). Lower coenostem effective transport distances ($ETD_{coenosteum}$) are associated with increased bleaching response (PCC = −0.603, $p = 0.022$, $n = 14$).

stress, as predicted by the optical feedback-loop hypothesis (Enríquez et al., 2005; Marcelino et al., 2013; Swain et al., 2016b; Wangpraseurt et al., 2017). Indeed, higher μ_{S,m_Ratio}' (i.e., $\mu_{s,m\_corallite}' > \mu_{s,m\_coenosteum}'$, PCC = 0.69, $p = 0.006$, $n = 14$) and lower $ETD_{coenosteum}$ (i.e., more effective transport, PCC = −0.603, $p = 0.022$, $n = 14$) are significantly associated with increased bleaching response among the coral species examined here. This pattern is consistent with the within-tissue micro-sensor measurements of Wangpraseurt et al. (2017), who demonstrated much larger increases in scalar irradiance enhancement within corallites than at either the coenosarc surface or oral surface of the polyps between bleached and non-bleached corals.

Using the light scattering properties and morphometrics of corallites and coenosteum, we then modeled the irradiance at the corallite surface due to light transport within the coenosteum, assuming that no other light hits the corallite and absorption is negligible (equations 4–8). The distribution of coenosteum-originated irradiance at the corallite surface ($R_{2\rightarrow1}(r)$) was modeled for three representative coral species with increasingly higher taxon-BRI and correspondingly progressively smaller $ETD_{coenosteum}$ (*Montastraea cavernosa, Seriatopora caliendrum,* and *Montipora informis,* **Figures 2**, **3A–C**). This can be quantified as the fraction of light that "escapes" the coenosteum and leaks into the corallite: $T_{2\rightarrow1} = \frac{\langle R_{2\rightarrow1}\rangle}{(\langle R_{2\rightarrow1}\rangle + \langle R_2\rangle)}$, where $\langle R_{2\rightarrow1}\rangle = \frac{1}{\pi r_c^2}\int_0^{r_c}\int_0^{2\pi} R_{2\rightarrow1}(r) r d\phi dr$ is the average irradiance at the corallite surface due to the light transported from the coenosteum and $\langle R_2\rangle = \frac{1}{\pi}\left(\left(r_c + l/2\right)^2 - r_c^2\right)\int_{r_c}^{r_c+l/2}\int_0^{2\pi} R_2(r) r d\phi dr$ is the average irradiance at the coenosteum. In case of *M. cavernosa* (high-$ETD_{coenosteum}$), only a small fraction of the coenosteum illumination reaches corallites (6%, **Table S3**). This fraction is much higher for the two species with more efficient light transport in the coenosteum (lower $ETD_{coenosteum}$); in *S. caliendrum,* and *M. informis*, nearly half of the light irradiating from the coenosteum gets transported into corallites (43 and 35%, respectively, **Table S3**). **Figures 3D,E** shows corresponding profiles of $R_{2\rightarrow1}$ as a function of the radial distance from the center of the corallites. In *M. cavernosa,* the species with the least efficient $ETD_{coenosteum}$ (low bleaching susceptibility, high-$ETD_{coenosteum}$), the small fraction of light that diffuses into the corallite stays in its periphery, hardly ever reaching the center ($\langle R_{2\rightarrow1}\rangle = 0.04$, **Figure 3D**). Conversely, corallites of the more efficient light transporters, *S. caliendrum* and *M. informis* (higher bleaching susceptibility and lower $ETD_{coenosteum}$) receive more light from the coenosteum, which also propagates further into the center of the corallites ($\langle R_{2\rightarrow1}\rangle = 0.07$ and $\langle R_{2\rightarrow1}\rangle = 0.2$, respectively, **Figures 3E,F**). Thus, *S. caliendrum* and *M. informis* corallites work as "light-trapping devices," diffusing light all the way through its center. This light-trapping effect of corallites is even more pronounced in *M. informis* which shows the highest bleaching susceptibility in our dataset (taxon-BRI = 73%, **Figure 3F**). Concomitantly, the fraction of the average corallite irradiance due light transport from the coenosteum, $F_{2\rightarrow1} = \frac{\langle R_{2\rightarrow1}\rangle}{(\langle R_{2\rightarrow1}\rangle + \langle R_2\rangle)}$, where $\langle R_1\rangle = \frac{1}{\pi} r_c^2 \int_0^{r_c}\int_0^{2\pi} R_1(r) r d\phi dr$, progressively increases from *M. cavernosa* to *S. caliendrum* and *M. informis*. While coenosteum-transported irradiance plays only a small role in the total irradiation of the corallites of *M. cavernosa* (5%, **Table S3**), the fraction is considerably higher for *S. caliendrum* (46%, **Table S3**), and *M. informis* corallites (64%, **Table S3**).

Both observational and simulated results suggest that higher μ_{S,m_Ratio}' and lower $ETD_{coenosteum}$ correlate with increased bleaching susceptibility in corals. The variable light environment between corallites and coenosarc is likely also a function of other effects, such as the spatially heterogeneous distribution of host pigments in the tissue; green fluorescent protein-like (GFP) pigments in the host are more abundant in polyps then in coenosarc (Salih et al., 2000; Kaniewska et al., 2011; Lyndby et al., 2016; Ong et al., 2018). Additionally, morphological plasticity in corals has been implicated in regulation of within-colony light levels to optimize light capture and photosynthesis (Kaniewska et al., 2008, 2014) and temperature microenvironments within the colony have been found to result from variations in colony morphology, irradiance, and flow patterns within and around the colony (Jimenez et al., 2011; Ong et al., 2017). Future work could look at the combined effect of tissue and skeleton in modulating light environment to the algae, in particular at the level of the polyp/corallite and coenosarc/coenosteum.

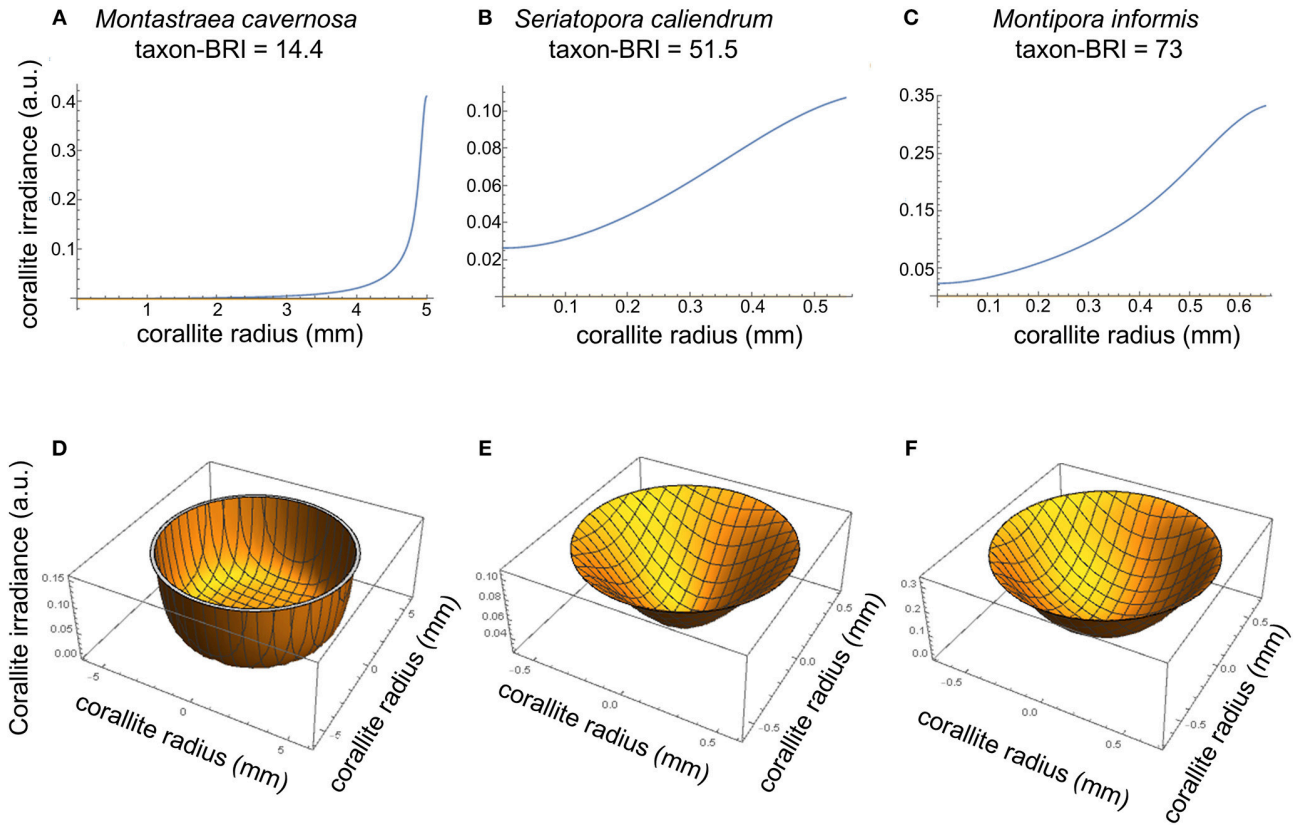

FIGURE 3 | Modeled irradiance at the corallite surface for *M. cavernosa* **(A,D)**, *S. caliendrum* **(B,E)** and *M. informis* **(C,F)** with increasing bleaching susceptibility scores (taxon-BRI of 14.4, 51.5, and 73, respectively) and differential $ETD_{coenosteum}$ and light scattering properties of both corallites and coenosteum (see **Figure 2** and **Table S3**). Plots of 2-D cross-sections through the middle of corallites **(A–C)** and 3-D top view cross-section representations of modeled irradiance in corallites due to light transport in the coenosteum **(D–F)**. The irradiance reaching the corallite was modeled as a function of the size of the corallite (mm), intercorallite distance (mm), and light scattering coefficient (μ_s') of corallite and coenosteum (equations 3–8).

Corals That Grow Faster Typically Have Lower Mass-Fractal Dimension, Denser Skeletons, Lower Skeletal Micro-μ_s' and Likely Show Higher Bleaching Susceptibility

Rate of deposition of calcium carbonate material (calcification rate) is the result of the linear extension of bio-aragonite deposited at the "centers of calcification" over time (linear growth or extension rate; mm yr^{-1}) and increased density from infilling by "thickening deposits" (bulk density or density of the deposited material and the volume of voids in the overall architecture; $gCaCO_3$ cm^{-3}) (reviewed in Stolarski, 2003; Cuif and Dauphin, 2005b; Lough and Cooper, 2011). The fractal coral growth model derived here relates linear extension rate of skeleton (G) and skeletal density (n) through a power-law (which has the property of invariance across a range of length-scales, thus representing fractal growth) with an exponent depending on D_f (Equations 3–7). Since $D_f < 3$ (Marcelino et al., 2013), the model showed that denser skeletons (i.e., higher n) tend to grow faster. This trend was confirmed by observational data with measured G and n for each coral species showing a positive correlation; branching and corymbose corals showed the highest skeletal density (1.94–2.33 $gCaCO_3$ cm^{-3}, $n = 26$) and linear extension rates (48.1–86.2 mm yr^{-1}) while massive, encrusting and columnar corals had the lowest skeletal density and linear extension rates (1.61–1.99 $gCaCO_3$ cm^{-3} and 12.38–20.44 mm yr^{-1}, $n = 29$; **Figure 4A**, $r = 0.35$, $p = 0.02$). These results agree with previously reported differences in growth strategies (i.e., higher investment in linear extension and/or skeletal density) which are due, in part, to the expected mechanical properties of different growth forms. Branching and digitate forms typically have higher extension rates and denser skeletons, while massive and encrusting forms show lower extension rates and lower skeletal density (Hughes, 1987; Jimenez and Cortes, 1993; Marshall, 2000; Morgan and Kench, 2012). However, rapidly growing branch tips of *Acropora* species are much less dense than their colony base due to secondary infilling of older parts of the colony to provide strength (Hughes, 1987; Bucher et al., 1998).

On average, dependence $G(n)$ followed a power-law form $G \propto n^{\alpha}$ with exponent $\alpha \sim 3.8$ (i.e., power law best fit to the experimental data). From Equation 13, $\alpha = \frac{1}{(3-D_f)}$, this exponent corresponds to the average value of $D_f \sim 2.74$,

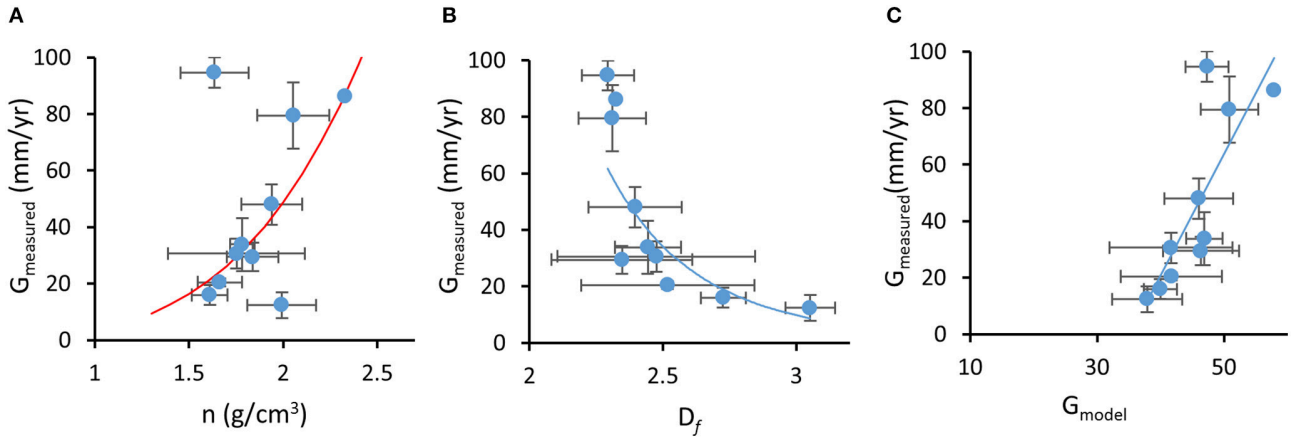

FIGURE 4 | Fractal coral growth model relating **(A)** measured growth (G) to measured skeletal density (*n*), where the red line represents model prediction, **(B)** measured growth to measured mass-fractal dimension (D_f), where the line represents power-law regression ($r^2 = 0.73$), and **(C)** measured growth to model-predicted growth, where the line represents linear regression ($r^2 = 0.67$). Error bars represent standard error.

which approximates the fractal dimension of diffusion-limited aggregation in three-dimensions (Peitgen et al., 1992). The model also predicts that G and D_f are inversely related: corals that exhibit faster linear growth rates are expected to form skeletons with lower fractal dimensions. This trend was also confirmed in our observational data with independently measured species-specific G and D_f averaged for each one of the 10 growth forms, which showed a significant negative correlation (in spite of the large variations in D_f for some growth forms, **Figure 4B**, $r = -0.30$, $p = 0.025$, $n = 59$). Furthermore, the fractal growth model was able to predict growth rates of coral taxa. We compared measured species-specific linear extension rates with linear extension rates predicted by the model (G in Equation 13) based on reported maximal skeletal density for each coral species and measured D_f for each coral skeleton. Although skeletal density is affected by processes that are not directly related to the linear fractal growth (e.g., infilling; Stolarski, 2003; Cuif and Dauphin, 2005b; Nothdurft and Webb, 2007), model-predicted G correlated well with measured growth rates (**Figure 4C**, $r = 0.39$, $p = 0.003$, $n = 59$). Additionally, the model prediction that skeletal density is inversely related to D_f was also validated ($r = 0.35$, $p = 0.009$, $n = 59$).

Predictions of the skeletal growth model, that corals with faster linear extension rates will have denser skeletons and will form skeletons with lower mass-fractal skeletal dimension, are in agreement with experimental data. D_f is one of the parameters that influence light scattering: according to light scattering theory (Rogers et al., 2014), $\mu_{s,m}{}'$ is expected to be proportional to D_f. This positive relationship between D_f and $\mu_{s,m}{}'$ was confirmed by our data (PCC = 0.224, $p = 0.036$, $n = 88$). Furthermore, the model shows inverse dependence between growth rate of the skeleton (i.e., linear extension rate) and the size of the biomineralized cluster R (Equation 13), which light theory describes as positively correlated with $\mu_{s,m}{}'$ (Rogers et al., 2009). Consequently, and although growth rate is influenced by several factors (reviewed in Dávalos-Dehullu et al., 2008; Lough and Cooper, 2011), the model predicts an inverse relationship between growth rate and $\mu_{s,m}{}'$, which is confirmed by our data (PCC = −0.292, $p = 0.017$). Since an inverse dependence between $\mu_{s,m}{}'$ and bleaching response has been shown through experimental and correlational evidence (Marcelino et al., 2013; Swain et al., 2016b), corals that grow faster are expected to have denser skeletons, lower skeletal D_f, lower $\mu_{s,m}{}'$, and are likely to show higher bleaching susceptibility. However, growth rate was not found to be significantly associated with bleaching susceptibility with phylogenetically-corrected regression analysis (**Table S2**) although taxon-BRI and measured G show an increasing linear relationship that plateaus (**Figure S1**).

Skeletal Structures of Varying Length Scales Known to Modulate the Light Microenvironment of Symbiodinium in Coral Tissue Are Not Associated With Bleaching Susceptibility

Several structures demonstrated to either directly modulate the internal light microenvironment, or to change in response to variation in external light fields at different length scales, were evaluated for possible association with bleaching susceptibility. Since $\mu_{s,m}{}'$ is inversely correlated with bleaching susceptibility (Marcelino et al., 2013; Swain et al., 2016b), we reasoned that skeletal structures that partially determine $\mu_{s,m}{}'$ could also conceivably be associated with bleaching susceptibility.

Micro-$\mu_s{}'$, similarly to light-scattering in tissue, is determined by interaction with several skeletal structures: (1) average size of nanograin (30–100 nm, Cuif and Dauphin, 2005a; Von Euw et al., 2017), and (2) extent of the fractal range in the biomineralized cluster R (which relate positively to $\mu_{s,m}{}'$; Rogers et al., 2009 and are currently unknown for individual species), (3) the shape of the optical refractive index correlation function C(r) given by mass-fractal dimension D_f (which inversely correlates with $\mu_{s,m}{}'$; Rogers et al., 2009) and was previously determined for

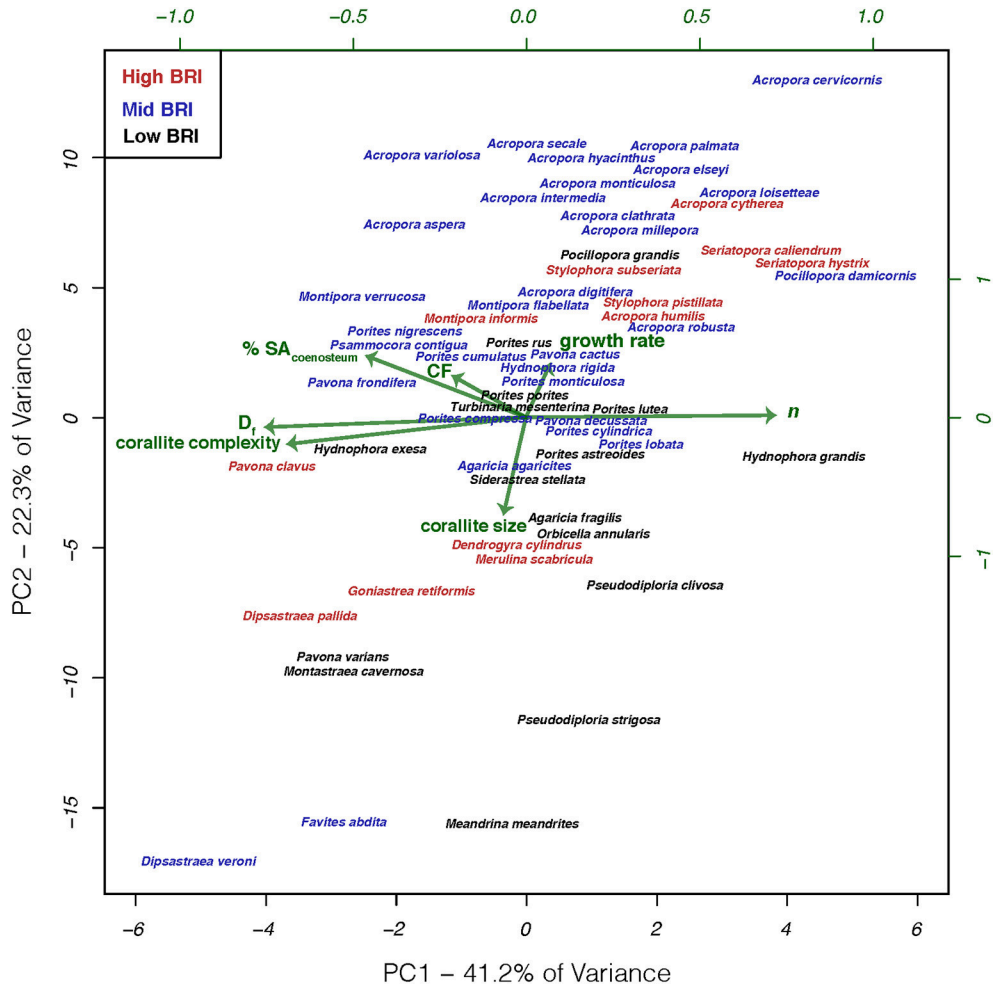

FIGURE 5 | Phylogenetic principal components analysis of characters thought to affect light microenvironments of *in hospite Symbiodinium* for 59 coral species. Phylogenetic correction based on the phylogeny modified from Huang (2012). Coral species color coded by bleaching response and arrows represent the relative contribution to each principal component.

all 88 targeted species (Marcelino et al., 2013), (4) the variance of the of the optical refractive index correlation function, *C(r)* (unknown for each species), and (5) macroscopic structures with voids (which will lower bulk- or micro-μ_s'; Enríquez et al., 2005; Stambler and Dubinsky, 2005; Rogers et al., 2009, 2014; Terán et al., 2010; Marcelino et al., 2013; and have been measured for some species).

Although D_f showed a significant association with $\mu_{s,m}'$ as expected from light theory, when D_f was tested for possible association with bleaching response, phylogenetically-corrected regression analysis revealed a non-significant negative relationship, indicating that although the mass-fractal organization of the skeleton is implicated in light scattering it is not correlated with bleaching susceptibility via the $\mu_{s,m}'$ pathway.

Macroscopic structures at higher length scales were also evaluated for possible association with bleaching susceptibility: colonial module dimensions (corallite size) and organization (corallite complexity, percent colony surface area composed of coenosteum—% $SA_{coenosteum}$). While it is clear that these features are related to each other in specific patterns across the coral phylogeny, since larger diameter corallites are also more complex (PCC = 0.809, $p < 0.001$, $n = 88$) and are surrounded by less coenosteum (PCC = −0.359, $p < 0.001$, $n = 88$; **Figure 1**; **Table S2**), none of these structures was significantly associated with bleaching response (**Figure 1**; **Table S2**). Finally, colony morphology (10 different growth forms listed in **Table S1**) was examined for correlation with bleaching susceptibility, since massive and encrusting colonies are historically reported to bleach and die at lower rates than branching and digitate colonies (Marshall and Baird, 2000; McClanahan, 2004; van Woesik et al., 2011).

We quantified each growth form by calculating *cumulative fractality*, or the product of the *apparent surface fractality* of each growth form, and D_f measured for each species. No significant correlation between taxon-BRI and *cumulative fractality* was detected (PCC = −0.08, $p = 0.47$, $n = 81$). We further performed phylo-log regression analysis on coral species that could be

classified as massive (coded as 0, $n = 44$) or branching (coded as 1, $n = 27$) and could not identify a significant association with bleaching response ($Z = -0.58$, $p = 0.56$). Additionally, we used growth form-specific ratios of surface area to volume described by Madin et al. (2016) (see **Text S2**) to quantify growth forms and also found no significant correlation with bleaching response. Recently it has been shown that the perceived relationship between growth forms and bleaching susceptibility is partially the result of their phylogentic relationships (McCowan et al., 2012; Swain et al., 2018); for example, while in the Faviidae family branching species bleached less than massive, the opposite was observed in the *Acroporidae* and *Poritidae* families (McCowan et al., 2012). Furthermore, due to the largely unknown effect of phenotypic plasticity within species (observed along gradients of light and nutrient flow) and species boundaries on colony morphology (reviewed in Veron, 2013), it has been challenging to accurately quantify and examine possible associations between species-specific growth forms and their bleaching response.

We reasoned that there may not be a clear relationship between bleaching response and individual features, but in combination with other skeletal characters known to modulate the light microenvironment, we may reveal their relationship with bleaching response. To that effect, we applied phylogenetically-corrected principal components analysis (phylo-PCA; **Figure 5**) to the seven characters that were not associated with taxon-BRI, to identify groups of characters that could be linearly combined in multi-dimensional space into principal components that explain the data variance: PC1 explained 41.2% and PC2 explained 22.3% of the data variance (PC3 explained only 15% of the data and was not considered further). Correlations between the two main principal components and the seven skeletal variables show that D_f, n, corallite complexity, and $\%\ SA_{coenosteum}$ were important components of PC1 while growth rate, corallite size and *cumulative fractality* were important components of PC2. Neither PC1 (PCC = 0.07, $p = 0.6$, $n = 59$) nor PC2 (PCC = 0.14, $p = 0.31$, $n = 59$) were significantly related to bleaching response.

These results show that variation in the skeletal structures targeted in this study, which have either been directly associated with modulating the light microenvironment surrounding *Symbiodinium* or shown to respond to variation in external light, are not related to bleaching response of these species. The lack of significant relationships should not be taken as an indication that these features do not actually modulate the internal light microenvironment of *in hospite Symbiodinium*, just that variation in these features and their abilities to modulate light microenvironments were not able to explain the observed variation in bleaching response across species. Variation in bleaching response among coral species has been attributed to diverse factors both intrinsic to the holobiont (e.g., thermotolerance of *Symbiodinium* and the interactions between coral, *Symbiodinium*, and other microbes; Baird et al., 2009; Leggat et al., 2011; Cunning and Baker, 2013; Krediet et al., 2013) and extrinsic from the environment (e.g., site-specific environmental conditions and frequency of thermal anomalies; McClanahan and Maina, 2003; Guest et al., 2012; Pratchett et al., 2013). Furthermore, the diversity of skeletal macro features observed among coral species are the result of simultaneous optimization of light capture and other vital functions including respiration and metabolite exchange between tissues and the environment (mass transfer; van Woesik et al., 2012), particle capture (Sebens et al., 1997), reproduction (Soong and Lang, 1992), and structural stability (Baldock et al., 2014). These forms are constrained by physical limitations imposed by the materials (Jimenez and Cortes, 1993; Boller et al., 2002) and three dimensional geometry of assembling modules (polyps) into a colony (Barbeitos, 2012), the physiological integration of those units (Coates and Oliver, 1973; Coates and Jackson, 1987; Soong and Lang, 1992 and Swain et al., 2018), and the evolutionary history of the species (Barbeitos et al., 2010; Budd et al., 2012). Perhaps the multitude of competing selection pressures directed at skeletal features may reveal correlations with bleaching susceptibility via pathways that are not light-scattering related, such as life-history strategies which have their own sets of specific morphological features (Darling et al., 2012, 2013). Corals with stress-tolerant strategies typically have massive morphologies, large corallites or meandroid polyp organization, grow slowly and have high fecundity, while corals with competitive strategies have large branching and plating morphologies, with smaller corallites, grow quickly, are more sensitive to storm breakages and bleach and die at greater rates during thermal stress events (Darling et al., 2012). Additionally, different morphologies are known to differ in their mass transfer abilities and within-tissue temperatures. Corals with higher surface area to volume ratios have faster gas and metabolite exchange across tissues (van Woesik et al., 2012), although ciliary movement (across the entire colony surface) can actively enhance mass transfer rates by 400% relative to passive molecular diffusion (Shapiro et al., 2014). Massive corals, due to their thick tissues and thicker thermal boundary layers, have higher within-tissue temperatures than branching corals with a thin veneer of tissue overlaying the skeleton and higher surface area to volume ratios (Jimenez et al., 2008, 2011). Furthermore, several non-photosynthetic fluorescent pigments present in host cells, such as GFP-like proteins, UV-absorbing compounds and other pigments, have been implicated in modulating the light microenvironment of *Symbiodinium* (Schlichter et al., 1986; Salih et al., 2000; Smith et al., 2013; Lyndby et al., 2016). In the case of GFP-like proteins, their role in modulating light microenvironment of *Symbiodinium* changes with pigment density. When present at low densities in the tissue, GFP-pigments scatter downwelling light, thus increasing light absorption and heating in the tissue, but at high pigment densities strong scattering reduces absorption and heating (Lyndby et al., 2016). The presence of GFP-pigments in the tissues may partially account for differential coral bleaching susceptibility and should be carefully investigated.

CONCLUSION

Skeletal light scattering, which has been shown to modulate the light microenvironment of *Symbiodinium* in coral tissue, is due to light interaction with structures ranging over several orders of

magnitude. Multiple lines of evidence predict that light scattering from the top ~200 μm (*micro-*μ_s') of skeleton is responsible for the rate of light increase to *Symbiodinium* and accelerated bleaching response to thermal stress (optical feedback-loop hypothesis). Here, phylogenetically-corrected regression analysis identified a relationship between *micro-*μ_s', but not bulk-μ_s' (light-scattering from the whole skeleton), and bleaching susceptibility in 88 coral species. Exploration of within-colony variation in *micro-*μ_s' in the 14-species subset, identified differences between *micro-*μ_s' of corallites and coenosteum, which can partially explain heterogeneity of light environments between polyp and coenosarc tissues. These results indicate that differential skeletal scattering between these structures could facilitate transport of light through the coenosteum to corallites which could then function as "photon-trapping" devices by repeatedly scattering photons off of septa and walls. Those species with inter-corallite spacing and skeletal optical properties that most facilitate this effect are the same species with elevated bleaching responses. However, when the size and complexity of corallites and the extent of coenosteum were measured, no correlation with bleaching could be identified. Furthermore, the well-known connection between colony morphology and bleaching response could not be verified, by either applying cumulative fractality or surface area to volume ratios as parameterizations of growth form, or by compiling growth forms into massive or branching groups in a phylogenetically-corrected regression. These results reveal the importance of performing phylogenetically-corrected correlations with skeletal characters that may otherwise closely reflect species evolutionary history and, as in the case of growth form, are also influenced by genetic and environmental factors. Finally, the effect of the fractal-like accretive growth of the skeleton on *micro-*μ_s' was examined by modeling growth as a function of density, size of nanograins, fractal range of biomineralized clusters, and overall mass-fractal dimension. The model, which was validated with experimental data, indicates that corals that grow faster typically have lower mass-fractal dimension, denser skeletons, lower skeletal micro-μ_s' and higher bleaching susceptibility. While this skeletal growth model was developed to estimate the average growth of skeleton at the colony-level, it should also be applicable to model growth of specific skeletal structures within the colony. Heterogeneity in calcification rates across skeletal structures have been observed in *Pocillopora damicornis* using nanoSIMS isotopic imaging, where skeletal extension in coenosteum is slower than corallite wall and dissepiments (Brahmi et al., 2012a,b). Future improvements to the model could account for this heterogenenous skeletal extension patterns to evaluate whether differences in calcification rates could potentially explain the difference between optical properties of coenosteum and corallites observed in this study.

AUTHOR CONTRIBUTIONS

LM, TS, and VB conceived and designed the research. HG, LM, NL, TS, and VB collected and compiled data. SL and TS performed phylogenetic analysis. LM, SL, TS, and VB analyzed the data and wrote the manuscript. All authors contributed to content revisions and approve of the final text.

FUNDING

This research was supported by the US National Science Foundation (EFRI-1240416 and CBET-1249311), and US National Institutes of Health (EB 003682).

ACKNOWLEDGMENTS

We thank R. Bieler and J. Gerber of the Field Museum for expertise and access to the FMNH museum collections and S. Cairns and T. Coffer of the National Museum of Natural History for expertise and access to the NMNH museum collections. Special thanks to D. Huang for providing us with the tree files for his comprehensive phylogeny of corals and M. Westneat for help analyzing them.

SUPPLEMENTARY MATERIAL

The Supplementary Material for this article can be found online at: https://www.frontiersin.org/articles/10.3389/fmars.2018.00450/full#supplementary-material

Figure S1 | Relationship between bleaching response and mean growth rate per growth form.

Table S1 | Character states and sources for each coral species.

Table S2 | Phylogenetically independent contrasts (PIC) analysis results.

Table S3 | Metrics quantifying the efficacy of the corallite irradiance due to light transport from the coenosteum (see section on "*Differences in Skeletal Micro-*μ_s' *of Corallites and Coenosteum Explain, in Part, Heterogeneous Light Environment Between Polyp and Coenosarc and are Associated With Bleaching Susceptibility*" for details).

Text S1 | Full references of **Table S1**.

Text S2 | Supplemental methods.

REFERENCES

Aizenberg, J., Weaver, J. C., Thanawala, M. S., Sundar, V. C., Morse, D. E., and Fratzl, P. (2005). Skeleton of *Euplectella* sp.: structural hierarchy from the nanoscale to the macroscale. *Science* 309, 275–278. doi: 10.1126/science.1112255

Allemand, D., Ferrier-Pages, C., Furla, P., Houlbreque, F., Puverel, S., Reynaud, S., et al. (2004). Biomineralisation in reef-building corals: from molecular mechanisms to environmental control. *Comptes Rendus Palevol* 3, 453–467. doi: 10.1016/j.crpv.2004.07.011

Anthony, K. R. N., and Hoegh-Guldberg, O. (2003). Variation in coral photosynthesis, respiration and growth characteristics in contrasting light microhabitats: an analogue to plants in forest gaps and understoreys? *Funct. Ecol.* 17, 246–259. doi: 10.1046/j.1365-2435.2003.00731.x

Anthony, K. R. N., Hoogenboom, M. O., and Connolly, S. R. (2005). Adaptive variation in coral geometry and the optimization of internal colony light climates. *Funct. Ecol.* 19, 17–26. doi: 10.1111/j.0269-8463.2005.00925.x

Baird, A. H., Bhagooli, R., Ralph, P. J., and Takahashi, S. (2009). Coral bleaching: the role of the host. *Trends Ecol. Evol.* 24, 16–20. doi: 10.1016/j.tree.2008.09.005

Baker, A. C., Glynn, P. W., and Riegl, B. (2008). Climate change and coral reef bleaching: an ecological assessment of long-term impacts, recovery trends and future outlook. *Estuar. Coast. Shelf Sci.* 80, 435–471. doi: 10.1016/j.ecss.2008.09.003

Baldock, T. E., Karampour, H., Sleep, R., Vyltla, A., Albermani, F., Golshani, A., et al. (2014). Resilience of branching and massive corals to wave loading under sea level rise—a coupled computational fluid dynamics-structural analysis. *Mar. Pollut. Bull.* 86, 91–101. doi: 10.1016/j.marpolbul.2014.07.038

Barbeitos, M. (2012). "Does polyp size constrain the morphological diversity of coral colonies?" in *12th International Coral Reef Symposium*, 30 (Cairns, QLD).

Barbeitos, M. S., Romano, S. L., and Lasker, H. R. (2010). Repeated loss of coloniality and symbiosis in scleractinian corals. *Proc. Natl. Acad. Sci. U.S.A.* 107, 11877–11882. doi: 10.1073/pnas.0914380107

Basillais, E. (1997). Coral surfaces and fractal dimensions: a new method. *Comptes Rendus Acad. Sci. Ser. III Sci. Vie* 320, 653–657.

Benzerara, K., Menguy, N., Obst, M., Stolarski, J., Mazur, M., Tylisczak, T., et al. (2011). Study of the crystallographic architecture of corals at the nanoscale by scanning transmission X-ray microscopy and transmission electron microscopy. *Ultramicroscopy* 111, 1268–1275. doi: 10.1016/j.ultramic.2011.03.023

Bhagooli, R., and Hidaka, M. (2004). Photoinhibition, bleaching susceptibility and mortality in two scleractinian corals, *Platygyra ryukyuensis* and *Stylophora pistillata*, in response to thermal and light stresses. *Comp. Biochem. Physiol. Part A* 137, 547–555. doi: 10.1016/j.cbpb.2003.11.008

Boller, M. L., Swain, T. D., and Lasker, H. R. (2002). Skeletal morphology and material properties of a fragmenting gorgonian coral. *Mar. Ecol. Prog. Ser.* 228, 131–141. doi: 10.3354/meps228131

Brahmi, C., Domart-Coulon, I., Rougee, L., Pyle, D. G., Stolarski, J., Mahoney, J. J., et al. (2012a). Pulsed 86Sr-labeling and NanoSIMS imaging to study coral biomineralization at ultra-structural length scales. *Coral Reefs* 31, 741–752. doi: 10.1007/s00338-012-0890-3

Brahmi, C., Kopp, C., Domart-Coulon, I., Stolarski, J., and Meibom, A. (2012b). Skeletal growth dynamics linked to trace-element composition in the scleractinian coral *Pocillopora damicornis*. *Geochim. Cosmochim. Acta* 99, 146–158. doi: 10.1016/j.gca.2012.09.031

Brodersen, K. E., Lichtenberg, M., Ralph, P. J., Kühl, M., and Wangpraseurt, D. (2014). Radiative energy budget reveals high photosynthetic efficiency in symbiont-bearing corals. *J. R. Soc. Interface* 11:20130997. doi: 10.1098/rsif.2013.0997

Bucher, D. J., Harriott, V. J., and Roberts, L. G. (1998). Skeletal micro-density, porosity and bulk density of acroporid corals. *J. Exp. Mar. Biol. Ecol.* 228, 117–136. doi: 10.1016/S0022-0981(98)00020-3

Budd, A. F., Fukami, H., Smith, N. D., and Knowlton, N. (2012). Taxonomic classification of the reef coral family Mussidae (Cnidaria: Anthozoa: Scleractinia). *Zool. J. Linn. Soc.* 166, 465–529. doi: 10.1111/j.1096-3642.2012.00855.x

Chindapol, N., Kaandorp, J. A., Cronemberger, C., Mass, T., and Genin, A. (2013). Modelling growth and form of the scleractinian coral *Pocillopora verrucosa* and the influence of hydrodynamics. *PLoS Comput. Biol.* 9:e1002849. doi: 10.1371/journal.pcbi.1002849

Coates, A. G., and Jackson, J. B. C. (1987). Clonal growth, algal symbiosis, and reef formation by corals. *Paleobiology* 13, 363–378. doi: 10.1017/S0094837300008988

Coates, A. G., and Oliver, W. A. J. (1973). "Coloniality in zoantharian corals," in *Animal Colonies: Development and Function Through Time*, eds R. S. Boardman, A. H. Cheetham, W. A. J. Oliver (Stroudsburg, PA: Hutchinson and Ross, Inc.), 3–27.

Cuif, J. P., and Dauphin, Y. (2005a). The environment recording unit in coral skeletons–a synthesis of structural and chemical evidences for a biochemically driven, stepping-growth process in fibres. *Biogeosciences* 2, 61–73. doi: 10.5194/bg-2-61-2005

Cuif, J. P., and Dauphin, Y. (2005b). The two-step mode of growth in the Scleractinian coral skeletons from the micrometre to the overall scale. *J. Struct. Biol.* 150, 319–331. doi: 10.1016/j.jsb.2005.03.004

Cunning, R., and Baker, A. C. (2013). Excess algal symbionts increase the susceptibility of reef corals to bleaching. *Nat. Clim. Chang.* 3, 259–262. doi: 10.1038/nclimate1711

Darling, E. S., Alvarez-Filip, L., Oliver, T. A., McClanahan, T. R., and Côté, I. M. (2012). Evaluating life-history strategies of reef corals from species traits. *Ecol. Lett.* 15, 1378–1386. doi: 10.1111/j.1461-0248.2012.01861.x

Darling, E. S., McClanahan, T. R., and Côté, I. M. (2013). Life histories predict coral community disassembly under multiple stressors. *Glob. Chang. Biol.* 19, 1930–1940. doi: 10.1111/gcb.12191

Dávalos-Dehullu, E., Hernández-Arana, H., and Carricart-Ganivet, J. P. (2008). On the causes of density banding in skeletons of corals of the genus *Montastraea*. *J. Exp. Mar. Biol. Ecol.* 365, 142–147. doi: 10.1016/j.jembe.2008.08.008

De Yoreo, J. J., Gilbert, P. U., Sommerdijk, N. A., Penn, R. L., Whitelam, S., Joester, D., et al. (2015). Crystallization by particle attachment in synthetic, biogenic, and geologic environments. *Science* 349:aaa6760. doi: 10.1126/science.aaa6760

Enríquez, S., Méndez, E. R., Hoegh-Guldberg, O., and Iglesias-Prieto, R. (2017). Key functional role of the optical properties of coral skeletons in coral ecology and evolution. *Proc. R. Soc. B Biol. Sci.* 284:20161667. doi: 10.1098/rspb.2016.1667

Enríquez, S., Méndez, E. R., and Iglesias-Prieto, R. (2005). Multiple scattering on coral skeletons enhances light absorption by symbiotic algae. *Limnol. Oceanogr.* 50, 1025–1032. doi: 10.4319/lo.2005.50.4.1025

Farris, J. S. (1989). The retention index and the rescaled consistency index. *Cladistics* 5, 417–419. doi: 10.1111/j.1096-0031.1989.tb00573.x

Frankowiak, K., Kret, S., Mazur, M., Meibom, A., Kitahara, M. V., and Stolarski, J. (2016). Fine-scale skeletal banding can distinguish symbiotic from asymbiotic species among modern and fossil scleractinian corals. *PLoS ONE* 11:e0147066. doi: 10.1371/journal.pone.0147066

Frieler, K., Meinshausen, M., Golly, A., Mengel, M., Lebek, K., Donner, S. D., et al. (2013). Limiting global warming to 2 degrees C is unlikely to save most coral reefs. *Nat. Clim. Chang.* 3, 165–170. doi: 10.1038/nclimate1674

Furukawa, Y., Nakajima, K., and Sato, K. (2001). *Advances in Crystal Growth Research*. New York, NY: Elsevier Science.

Guest, J. R., Baird, A. H., Maynard, J. A., Muttaqin, E., Edwards, A. J., Campbell, S. J., et al. (2012). Contrasting patterns of coral bleaching susceptibility in 2010 suggest an adaptive response to thermal stress. *PLoS ONE* 7:e33353. doi: 10.1371/journal.pone.0033353

Ho, L. s., and Ané, C. (2014). A linear-time algorithm for Gaussian and non-Gaussian trait evolution models. *Syst. Biol.* 63, 397–408. doi: 10.1093/sysbio/syu005

Hoegh-Guldberg, O., Mumby, P. J., Hooten, A. J., Steneck, R. S., Greenfield, P., Gomez, E., et al. (2007). Coral reefs under rapid climate change and ocean acidification. *Science* 318, 1737–1742. doi: 10.1126/science.1152509

Huang, D. (2012). Threatened reef corals of the world. *PLoS ONE* 7:e34459. doi: 10.1371/journal.pone.0034459

Hughes, T. P. (1987). Skeletal density and growth form of corals. *Mar. Ecol. Prog. Ser.* 35, 259–266. doi: 10.3354/meps035259

Hughes, T. P., Kerry, J. T., Álvarez-Noriega, M., Álvarez-Romero, J. G., Anderson, K. D., Baird, A. H., et al. (2017). Global warming and recurrent mass bleaching of corals. *Nature* 543, 373–377. doi: 10.1038/nature21707

Iglesias-Prieto, R., Matta, J. L., Robins, W. A., and Trench, R. K. (1992). Photosynthetic response to elevated temperature in the symbiotic dinoflagellate *Symbiodinium microadriaticum* in culture. *Proc. Natl. Acad. Sci. USA.* 89, 10302–10305. doi: 10.1073/pnas.89.21.10302

Ishimaru, A. (1999). *Wave Propagation and Scattering in Random Media*. New York, NY: Wiley-IEEE Press.

Ivens, A. B., von Beeren, C., Blüthgen, N., and Kronauer, D. J. (2016). Studying the complex communities of ants and their symbionts using ecological network analysis. *Annu. Rev. Entomol.* 61, 353–371. doi: 10.1146/annurev-ento-010715-023719

Ives, A. R., and Garland, T. (2010). Phylogenetic logistic regression for binary dependent variables. *Syst. Biol.* 59, 9–26. doi: 10.1093/sysbio/syp074

Jimenez, C., and Cortes, J. (1993). Density and compressive strength of the coral *Siderastrea siderea* (Scleractinia, Siderastreidae): intraspecific variability. *Rev. Biol. Trop.* 41, 39–43.

Jimenez, I. M., Kühl, M., Larkum, A. W., and Ralph, P. J. (2011). Effects of flow and colony morphology on the thermal boundary layer of corals. *J. R. Soc. Interface* 8, 1785–1795. doi: 10.1098/rsif.2011.0144

Jimenez, I. M., Kühl, M., Larkum, A. W. D., and Ralph, P. J. (2008). Heat budget and thermal microenvironment of shallow-water corals: do massive corals get warmer than branching corals? *Limnol. Oceanogr.* 53, 1548–1561. doi: 10.4319/lo.2008.53.4.1548

Jokiel, P. L. (2004). "Temperature stress and coral bleaching," in *Coral Health and Disease*, eds E. Rosenberg, Y. Loya (Berlin, Heidelberg: Springer-Verlag), 401–425.

Jones, R. J. (2008). Coral bleaching, bleaching-induced mortality, and the adaptive significance of the bleaching response. *Mar. Biol.* 154, 65–80. doi: 10.1007/s00227-007-0900-0

Kaandorp, J. A., Sloot, P. M., Merks, R. M., Bak, R. P., Vermeij, M. J., and Maier, C. (2005). Morphogenesis of the branching reef coral *Madracis mirabilis*. *Proc. R. Soc. B Biol. Sci.* 272, 127–133. doi: 10.1098/rspb.2004.2934

Kahng, S. E., Hochberg, E. J., Apprill, A., Wagner, D., Luck, D. G., Perez, D., et al. (2012). Efficient light harvesting in deep-water zooxanthellate corals. *Mar. Ecol. Prog. Ser.* 455, 65–77. doi: 10.3354/meps09657

Kamat, S., Su, X., Ballarini, R., and Heuer, A. H. (2000). Structural basis for the fracture toughness of the shell of the conch *Strombus gigas*. *Nature* 405, 1036–1040. doi: 10.1038/35016535

Kaniewska, P., Anthony, K. R. N., and Hoegh-Guldberg, O. (2008). Variation in colony geometry modulates internal light levels in branching corals *Acropora humilis* and *Stylophora pistillata*. *Mar. Biol.* 155, 649–660. doi: 10.1007/s00227-008-1061-5

Kaniewska, P., Anthony, K. R. N., Sampayo, E. M., Campbell, P. R., and Hoegh-Guldberg, O. (2014). Implications of geometric plasticity for maximizing photosynthesis in branching corals. *Mar. Biol.* 161, 313–328. doi: 10.1007/s00227-013-2336-z

Kaniewska, P., Magnusson, S. H., Anthony, K. R. N., Reef, R., Kühl, M., and Hoegh-Guldberg, O. (2011). Importance of macro-versus microstructure in modulating light levels inside coral colonies. *J. Phycol.* 47, 846–860. doi: 10.1111/j.1529-8817.2011.01021.x

Kim, Y. L., Liu, Y., Turzhitsky, V. M., Roy, H. K., Wali, R. K., and Backman, V. (2004). Coherent backscattering spectroscopy. *Opt. Lett.* 29, 1906–1908. doi: 10.1364/OL.29.001906

Klaus, J. S., Budd, A. F., Heikoop, J. M., and Fouke, B. W. (2007). Environmental controls on corallite morphology in the reef coral *Montastraea annularis*. *Bull. Mar. Sci.* 80, 233–260. Available online at: https://www.ingentaconnect.com/contentone/umrsmas/bullmar/2007/00000080/00000001/art00015#expand/collapse

Krediet, C. J., Ritchie, K. B., Paul, V. J., and Teplitski, M. (2013). Coral-associated micro-organisms and their roles in promoting coral health and thwarting diseases. *Proc. R. Soc. B Biol. Sci.* 280:20122328. doi: 10.1098/rspb.2012.2328

Kühl, M., Cohen, Y., Dalsgaard, T., Jorgensen, B. B., and Revsbech, NP (1995). Microenvironment and photosynthesis of zooxanthellae in scleractinian corals studied with microsensors for O_2, pH and Light. *Mar. Ecol. Prog. Ser.* 117, 159–172. doi: 10.3354/meps117159

Leggat, W., Seneca, F., Wasmund, K., Ukani, L., Yellowlees, D., and Ainsworth, T. D. (2011). Differential responses of the coral host and their algal symbiont to thermal stress. *PLoS ONE* 6:e26687. doi: 10.1371/journal.pone.0026687

Lesser, M. P., and Farrell, J. H. (2004). Exposure to solar radiation increases damage to both host tissues and algal symbionts of corals during thermal stress. *Coral Reefs* 23, 367–377. doi: 10.1007/s00338-004-0392-z

Lichtenberg, M., Larkum, A. W., and Kühl, M. (2016). Photosynthetic acclimation of *Symbiodinium in hospite* depends on vertical position in the tissue of the scleractinian coral *Montastrea curta*. *Front. Microbiol.* 7:230. doi: 10.3389/fmicb.2016.00230

Lough, J. M., and Cooper, T. F. (2011). New insights from coral growth band studies in an era of rapid environmental change. *Earth Sci. Rev.* 108, 170–184. doi: 10.1016/j.earscirev.2011.07.001

Loya, Y., Sakai, K., Yamazato, K., Nakano, Y., Sambali, H., and van Woesik, R. (2001). Coral bleaching: the winners and the losers. *Ecol. Lett.* 4, 122–131. doi: 10.1046/j.1461-0248.2001.00203.x

Lyndby, N. H., Kühl, M., and Wangpraseurt, D. (2016). Heat generation and light scattering of green fluorescent protein-like pigments in coral tissue. *Sci. Rep.* 6:26599. doi: 10.1038/srep26599

Maddison, W. P., and Maddison, D. R. (2011). *Mesquite: A Modular System for Evolutionary Analysis*. Available online at: http://mesquiteproject.org

Madin, J. S., Hoogenboom, M. O., Connolly, S. R., Darling, E. S., Falster, D. S., Huang, D. W., et al. (2016). A trait-based approach to advance coral reef science. *Trends Ecol. Evol.* 31, 419–428. doi: 10.1016/j.tree.2016.02.012

Magnusson, S. H., Fine, M., and Kühl, M. (2007). Light microclimate of endolithic phototrophs in the scleractinian corals *Montipora monasteriata* and *Porites cylindrica*. *Mar. Ecol. Prog. Ser.* 332, 119–128. doi: 10.3354/meps332119

Marcelino, L. A., Westneat, M. W., Stoyneva, V., Henss, J., Rogers, J. D., Radosevich, A., et al. (2013). Modulation of light-enhancement to symbiotic algae by light-scattering in corals and evolutionary trends in bleaching. *PLoS ONE* 8:e61492. doi: 10.1371/journal.pone.0061492

Marshall, P. A. (2000). Skeletal damage in reef corals: relating resistance to colony morphology. *Mar. Ecol. Prog. Ser.* 200, 177–189. doi: 10.3354/meps200177

Marshall, P. A., and Baird, A. H. (2000). Bleaching of corals on the Great Barrier Reef: differential susceptibilities among taxa. *Coral Reefs* 19, 155–163. doi: 10.1007/s003380000086

Martin-Garin, B., Lathuiliére, B., Verrecchia, E. P., and Geister, J. (2007). Use of fractal dimensions to quantify coral shape. *Coral Reefs* 26, 541–550. doi: 10.1007/s00338-007-0256-4

McClanahan, T. R. (2004). The relationship between bleaching and mortality of common corals. *Mar. Biol.* 144, 1239–1245. doi: 10.1007/s00227-003-1271-9

McClanahan, T. R., and Maina, J. (2003). Response of coral assemblages to the interaction between natural temperature variation and rare warm-water events. *Ecosystems* 6, 551–563. doi: 10.1007/s10021-002-0104-x

McCowan, D. M., Pratchett, M. S., and Baird, A. H. (2012). "Bleaching susceptibility and mortality among corals with differing growth forms," in *12th International Coral Reef Symposium*. Vol. 9A (Cairns, QLD), 1–6.

Midford, P. E., Garland, T Jr, and Maddison, W. P. (2010). *PDAP Package*. Available online at: http://mesquiteproject.org

Miyashita, S., Saito, Y., and Uwaha, M. (2005). Fractal aggregation growth and the surrounding diffusion field. *J. Cryst. Growth* 283, 533–539. doi: 10.1016/j.jcrysgro.2005.05.074

Morgan, K. M., and Kench, P. S. (2012). Skeletal extension and calcification of reef-building corals in the central Indian Ocean. *Mar. Environ. Res.* 81, 78–82. doi: 10.1016/j.marenvres.2012.08.001

Muko, S., Kawasaki, K., Sakai, K., Takasu, F., and Shigesada, N. (2000). Morphological plasticity in the coral *Porites sillimaniani* and its adaptive significance. *Bull. Mar. Sci.* 66, 225–239. Available online at: https://www.ingentaconnect.com/search/article?option1=tka&value1=Morphological+plasticity+in+the+coral+Porites+sillimaniani+and+its+adaptive&pageSize=10&index=1

Mumby, P. J., Chisholm, J. R. M., Edwards, A. J., Andrefouet, S., and Jaubert, J. (2001). Cloudy weather may have saved Society Island reef corals during the 1998 ENSO event. *Mar. Ecol. Prog. Ser.* 222, 209–216. doi: 10.3354/meps222209

Muscatine, L. (1990). "The role of symbiotic algae in carbon and energy flux in reef corals," in *Coral Reefs*, ed Z. Dubinsky (Amsterdam: Elsevier), 75–87.

Nir, O., Gruber, D. F., Einbinder, S., Kark, S., and Tchernov, D. (2011). Changes in scleractinian coral *Seriatopora hystrix* morphology and its endocellular *Symbiodinium* characteristics along a bathymetric gradient from shallow to mesophotic reef. *Coral Reefs* 30, 1089–1100. doi: 10.1007/s00338-011-0801-z

Nothdurft, L. D., and Webb, G. E. (2007). Microstructure of common reef-building coral genera *Acropora*, *Pocillopora*, *Goniastrea* and *Porites*: constraints on spatial resolution in geochemical sampling. *Facies* 53, 1–26. doi: 10.1007/s10347-006-0090-0

Ong, R. H., King, A. J. C., Caley, M. J., and Mullins, B. J. (2018). Prediction of solar irradiance using ray-tracing techniques for coral macro- and micro-habitats. *Mar. Environ. Res.* 141, 75–87. doi: 10.1016/j.marenvres.2018.08.004

Ong, R. H., King, A. J. C., Kaandorp, J. A., Mullins, B. J., and Caley, M. J. (2017). The effect of allometric scaling in coral thermal microenvironments. *PLoS ONE* 12:e0184214. doi: 10.1371/journal.pone.0184214

Ow, Y. X., and Todd, P. A. (2010). Light-induced morphological plasticity in the scleractinian coral *Goniastrea pectinata* and its functional significance. *Coral Reefs* 29, 797–808. doi: 10.1007/s00338-010-0631-4

Peitgen, H.-O., Jürgens, H., and Saupe, D. (1992). *Chaos and Fractals: New Frontiers of Science*. New York, NY: Springer-Verlag. doi: 10.1007/978-1-4757-4740-9

Pochon, X., Forsman, Z. H., Spalding, H. L., Padilla-Gamiño, J. L., Smith, C. M., and Gates, R. D. (2015). Depth specialization in mesophotic corals (*Leptoseris* spp.) and associated algal symbionts in Hawai'i. *R. Soc. Open Sci.* 2, 1–14. doi: 10.1098/rsos.140351

Pratchett, M. S., McCowan, D., Maynard, J. A., and Heron, S. F. (2013). Changes in bleaching susceptibility among corals subject to ocean warming and recurrent bleaching in Moorea, French Polynesia. *PLoS ONE* 8:e70443. doi: 10.1371/journal.pone.0070443

Przeniosło, R., Stolarski, J., Mazur, M., and Brunelli, M. (2008). Hierarchically structured scleractinian coral biocrystals. *J. Struct. Biol.* 161, 74–82. doi: 10.1016/j.jsb.2007.09.020

Ralph, P. J., Gademann, R., Larkum, A. W. D., and Kühl, M. (2002). Spatial heterogeneity in active chlorophyll fluorescence and PSII activity of coral tissues. *Mar. Biol.* 141, 639–646. doi: 10.1007/s00227-002-0866-x

Revell, L. J. (2009). Size-correction and principal components for interspecific comparative studies. *Evolution* 63, 3258–3268. doi: 10.1111/j.1558-5646.2009.00804.x

Revell, L. J. (2010). Phylogenetic signal and linear regression on species data. *Methods Ecol. Evol.* 1, 319–329. doi: 10.1111/j.2041-210X.2010.00044.x

Revell, L. J. (2012). Phytools: an R package for phylogenetic comparative biology (and other things). *Methods Ecol. Evol.* 3, 217–223. doi: 10.1111/j.2041-210X.2011.00169.x

Rezende, E. L., Lavabre, J. E., Guimarães, P. R., Jordano, P., and Bascompte, J. (2007). Non-random coextinctions in phylogenetically structured mutualistic networks. *Nature* 448, U925–U926. doi: 10.1038/nature05956

Rocha, R. J., Silva, A. M., Fernandes, M. H., Cruz, I. C., Rosa, R., and Calado, R. (2014). Contrasting light spectra constrain the macro and microstructures of scleractinian corals. *PLoS ONE* 9:e105863. doi: 10.1371/journal.pone.0105863

Rodríguez-Roman, A., Hernández-Pech, X., Thomé, P. E., Enríquez, S., and Iglesias-Prieto, R. (2006). Photosynthesis and light utilization in the Caribbean coral *Montastraea faveolata* recovering from a bleaching event. *Limnol. Oceanogr.* 51, 2702–2710. doi: 10.4319/lo.2006.51.6.2702

Rogers, J. D., and Capoglu, I. R., Backman, V. (2009). Nonscalar elastic light scattering from continuous random media in the Born approximation. *Opt. Lett.* 34, 1891–1893. doi: 10.1364/OL.34.001891

Rogers, J. D., Radosevich, A. J., Yi, J., and Backman, V. (2014). Modeling light scattering in tissue as continuous random media using a versatile refractive index correlation function. *IEEE J. Select. Top. Quant. Electronics* 20, 173–186. doi: 10.1109/jstqe.2013.2280999

Salih, A., Larkum, A., Cox, G., Kühl, M., and Hoegh-Guldberg, O. (2000). Fluorescent pigments in corals are photoprotective. *Nature* 408, 850–853. doi: 10.1038/35048564

Schlichter, D., Fricke, H. W., and Weber, W. (1986). Light harvesting by wavelength transformation in a symbiotic coral of the Red Sea twilight zone. *Mar. Biol.* 91, 403–407. doi: 10.1007/BF00428634

Sebens, K. P., Witting, J., and Helmuth, B. (1997). Effects of water flow and branch spacing on particle capture by the reef coral *Madracis mirabilis* (Duchassaing and Michelotti). *J. Exp. Mar. Biol. Ecol.* 211, 1–28. doi: 10.1016/S0022-0981(96)02636-6

Shapiro, O. H., Fernandez, V. I., Garren, M., Guasto, J. S., Debaillon-Vesque, F. P., Kramarsky-Winter, E., et al. (2014). Vortical ciliary flows actively enhance mass transport in reef corals. *Proc. Natl. Acad. Sci. USA.* 111, 13391–13396. doi: 10.1073/pnas.1323094111

Smith, E. G., D'Angelo, C., Salih, A., and Wiedenmann, J. (2013). Screening by coral green fluorescent protein (GFP)-like chromoproteins supports a role in photoprotection of zooxanthellae. *Coral Reefs* 32, 463–474. doi: 10.1007/s00338-012-0994-9

Smith, L. W., and Birkeland, C. (2007). Effects of intemittent flow and irradiance level on back reef *Porites* corals at elevated seawater temperatures. *J. Exp. Mar. Biol. Ecol.* 341, 282–294. doi: 10.1016/j.jembe.2006.10.053

Soong, K., and Lang, J. C. (1992). Reproductive integration in reef corals. *Biol. Bull.* 183, 418–431. doi: 10.2307/1542018

Stambler, N., and Dubinsky, Z. (2005). Corals as light collectors: an integrating sphere approach. *Coral Reefs* 24, 1–9. doi: 10.1007/s00338-004-0452-4

Stolarski, J. (2003). Three-dimensional micro- and nanostructural characteristics of the scleractinian coral skeleton: a biocalcification proxy. *Acta Palaeontol. Pol.* 48, 497–530.

Stolarski, J., and Mazur, M. (2005). Nanostructure of biogenic versus abiogenic calcium carbonate crystals. *Acta Palaeontol. Pol.* 50, 847–865. Available online at: https://www.app.pan.pl/article/item/app50-847.html

Swain, T. D., Bold, E. C., Osborn, P. C., Baird, A. H., Westneat, M. W., Backman, V., et al. (2018). Physiological integration of coral colonies is correlated with bleaching resistance. *Mar. Ecol. Prog. Ser.* 586, 1–10. doi: 10.3354/meps12445

Swain, T. D., DuBois, E., Gomes, A., Stoyneva, V. P., Radosevich, A. J., Henss, J., et al. (2016b). Skeletal light-scattering accelerates bleaching response in reef-building corals. *BMC Ecol.* 16:10. doi: 10.1186/s12898-016-0061-4

Swain, T. D., Vega-Perkins, J. B., Oestreich, W. K., Triebold, C., DuBois, E., Henss, J., et al. (2016a). Coral bleaching response index: a new tool to standardize and compare susceptibility to thermal bleaching. *Glob. Chang. Biol.* 22, 2475–2488. doi: 10.1111/gcb.13276

Terán, E., Méndez, E. R., Enríquez, S., and Iglesias-Prieto, R. (2010). Multiple light scattering and absorption in reef-building corals. *Appl. Opt.* 49, 5032–5042. doi: 10.1364/AO.49.005032

Todd, P. A. (2008). Morphological plasticity in scleractinian corals. *Biol. Rev.* 83, 315–337. doi: 10.1111/j.1469-185X.2008.00045.x

Todd, P. A., Ladle, R. J., Lewin-Koh, N. J. I., and Chou, L. M. (2004). Genotype x environment interactions in transplanted clones of the massive corals *Favia speciosa* and *Diploastrea helippora*. *Mar. Ecol. Prog. Ser.* 271, 167–182. doi: 10.3354/meps271167

Ulstrup, K. E., Ralph, P. J., Larkum, A. W. D., and Kühl, M. (2006). Intra-colonial variability in light acclimation of zooxanthellae in coral tissues of *Pocillopora damicornis*. *Mar. Biol.* 149, 1325–1335. doi: 10.1007/s00227-006-0286-4

Ulstrup, K. E., van Oppen, M. J. H., Kühl, M., and Ralph, P. J. (2007). Inter-polyp genetic and physiological characterisation of *Symbiodinium* in an *Acropora valida* colony. *Mar. Biol.* 153, 225–234. doi: 10.1007/s00227-007-0806-x

Uwaha, M., and Saito, Y. (1990). Fractal aggregation and dendritic crystal-growth. *J. Cryst. Growth* 99, 175–178. doi: 10.1016/0022-0248(90)90507-H

van Woesik, R., Irikawa, A., Anzai, R., and Nakamura, T. (2012). Effects of coral colony morphologies on mass transfer and susceptibility to thermal stress. *Coral Reefs* 31, 633–639. doi: 10.1007/s00338-012-0911-2

van Woesik, R., Sakai, K., Ganase, A., and Loya, Y. (2011). Revisiting the winners and the losers a decade after coral bleaching. *Mar. Ecol. Prog. Ser.* 434, 67–76. doi: 10.3354/meps09203

Veron, J. (2013). Overview of the taxonomy of zooxanthellate Scleractinia. *Zool. J. Linn. Soc.* 169, 485–508. doi: 10.1111/zoj.12076

Von Euw, S., Zhang, Q., Manichev, V., Murali, N., Gross, J., Feldman, L. C., et al. (2017). Biological control of aragonite formation in stony corals. *Science* 356, 933–938. doi: 10.1126/science.aam6371

Wangpraseurt, D., Holm, J. B., Larkum, A. W., Pernice, M., Ralph, P. J., Suggett, D. J., et al. (2017). *In vivo* microscale measurements of light and photosynthesis during coral bleaching: evidence for the optical feedback loop? *Front. Microbiol.* 8:59. doi: 10.3389/fmicb.2017.00059

Wangpraseurt, D., Jacques, S. L., Petrie, T., and Kühl, M. (2016). Monte Carlo modeling of photon propagation reveals highly scattering coral tissue. *Front. Plant Sci.* 7:1404. doi: 10.3389/fpls.2016.01404

Wangpraseurt, D., Larkum, A. W. D., Franklin, J., Szabó, M., Ralph, P. J., and Kühl, M. (2014a). Lateral light transfer ensures efficient resource distribution in symbiont-bearing corals. *J. Exp. Biol.* 217, 489–498. doi: 10.1242/jeb.091116

Wangpraseurt, D., Larkum, A. W. D., Ralph, P. J., and Kühl, M. (2012). Light gradients and optical microniches in coral tissues. *Front. Microbiol.* 3:316. doi: 10.3389/fmicb.2012.00316

Wangpraseurt, D., Polerecky, L., Larkum, A. W. D., Ralph, P. J., Nielsen, D. A., Pernice, M., et al. (2014b). The *in situ* light microenvironment

of corals. *Limnol. Oceanogr.* 59, 917–926. doi: 10.4319/lo.2014.59.3.0917

Warner, M. E., Fitt, W. K., and Schmidt, G. W. (1999). Damage to photosystem II in symbiotic dinoflagellates: a determinant of coral bleaching. *Proc. Natl. Acad. Sci. U.S.A.* 96, 8007–8012. doi: 10.1073/pnas.96.14.8007

Young, G. C., Dey, S., Rogers, A. D., and Exton, D. (2017). Cost and time-effective method for multi-scale measures of rugosity, fractal dimension, and vector dispersion from coral reef 3D models. *PLoS ONE* 12:e0175341. doi: 10.1371/journal.pone.0175341

Zhang, H., Gao, S., Lercher, M. J., Hu, S., and Chen, W. H. (2012). EvolView, an online tool for visualizing, annotating and managing phylogenetic trees. *Nucleic Acids Res.* 40, W569–W572. doi: 10.1093/nar/gks576

Zonios, G., Perelman, L. T., Backman, V., Manoharan, R., Fitzmaurice, M., Van Dam, J., et al. (1999). Diffuse reflectance spectroscopy of human adenomatous colon polyps *in vivo*. *Appl. Opt.* 38, 6628–6637. doi: 10.1364/AO.38.006628

Conflict of Interest Statement: The authors declare that the research was conducted in the absence of any commercial or financial relationships that could be construed as a potential conflict of interest.

Copyright © 2018 Swain, Lax, Lake, Grooms, Backman and Marcelino. This is an open-access article distributed under the terms of the Creative Commons Attribution License (CC BY). The use, distribution or reproduction in other forums is permitted, provided the original author(s) and the copyright owner(s) are credited and that the original publication in this journal is cited, in accordance with accepted academic practice. No use, distribution or reproduction is permitted which does not comply with these terms.